Molecular Therapy
Original Article

Treatment with THI, an inhibitor of sphingosine-1-phosphate lyase, modulates glycosphingolipid metabolism and results therapeutically effective in experimental models of Huntington's disease

Giuseppe Pepe,[1] Luca Capocci,[1] Federico Marracino,[1] Natalia Realini,[2] Paola Lenzi,[3] Katiuscia Martinello,[1] Tiziana Francesca Bovier,[4,5,6] Terry Jo Bichell,[7,11] Pamela Scarselli,[1] Clotilde Di Cicco,[1] Aaron B. Bowman,[8] Filomena A. Digilio,[4] Sergio Fucile,[1,9] Francesco Fornai,[1,3] Andrea Armirotti,[2] Rosanna Parlato,[10] Alba Di Pardo,[1] and Vittorio Maglione[1]

[1]IRCCS Neuromed, Pozzilli (IS) 86077, Italy; [2]Analytical Chemistry Lab, Fondazione Istituto Italiano di Tecnologia, Via Morego 30, 16163 Genoa, Italy; [3]Department of Translational Research and New Technologies in Medicine and Surgery, University of Pisa, Via Roma 55, 56126 Pisa, Italy; [4]Research Institute on Terrestrial Ecosystems (IRET), UOS Naples-CNR, Via Pietro Castellino 111, 80131 Naples, Italy; [5]Department of Pediatrics Columbia University Vagelos College of Physicians and Surgeons, New York, NY 10032, USA; [6]Center for Host–Pathogen Interaction, Columbia University Vagelos College of Physicians and Surgeons, New York 10032, NY, USA; [7]Vanderbilt Brain Institute, Vanderbilt University, Nashville, TN 37240, USA; [8]School of Health Sciences, Purdue University, West Lafayette, IN 47907-2051, USA; [9]Department of Physiology and Pharmacology, Sapienza Rome University, Rome 00185, Italy; [10]Division for Neurodegenerative Diseases, Department of Neurology, Mannheim Center for Translational Neuroscience, Medical Faculty Mannheim Heidelberg University, Mannheim 68167, Germany

Huntington's disease (HD) is a fatal neurodegenerative disorder with no effective cure currently available. Over the past few years our research has shown that alterations in sphingolipid metabolism represent a critical determinant in HD pathogenesis. In particular, aberrant metabolism of sphingosine-1-phosphate (S1P) has been reported in multiple disease settings, including human postmortem brains from HD patients. In this study, we investigate the potential therapeutic effect of the inhibition of S1P degradative enzyme SGPL1, by the chronic administration of the 2-acetyl-5-tetrahydroxybutyl imidazole (THI) inhibitor. We show that THI mitigated motor dysfunctions in both mouse and fly models of HD. The compound evoked the activation of pro-survival pathways, normalized levels of brain-derived neurotrophic factor, preserved white matter integrity, and stimulated synaptic functions in HD mice. Metabolically, THI restored normal levels of hexosylceramides and stimulated the autophagic and lysosomal machinery, facilitating the reduction of nuclear inclusions of both wild-type and mutant huntingtin proteins.

INTRODUCTION

Huntington's disease (HD) is the most common dominantly inherited neurodegenerative disorder characterized by the progressive striatal and cortical degeneration and associated motor, cognitive, and behavioral disturbances.[1] The disease-causing mutation is a polyglutamine (polyQ) stretch within the N-terminal of huntingtin (Htt), a ubiquitously expressed and brain-enriched protein that plays a role in multiple cellular pathways.[2]

When mutated, Htt exerts a variety of undesirable toxic effects in both neuronal and non-neuronal cells[1,3,4] and interferes with cellular metabolism at multiple levels.[5–7]

Among all the metabolic dysfunctions associated with HD, alterations in the metabolism of some glycosphingolipid species (gangliosides) seem to contribute to its pathogenesis.[8–11] Decreased gene expression of specific ganglioside-metabolizing enzymes has been described in multiple HD pre-clinical models and in HD patients.[8,9,12] Increasing evidence indicates that expression of enzymes controlling the metabolism of some other sphingolipids is also aberrant in HD and it may represent a potential therapeutic target.[13–17] In particular, sphingosine-1-phosphate (S1P) metabolism has been described to be dysfunctional in multiple HD experimental models as well as in HD human postmortem brain tissues.[17-20]

S1P is one of the most potent signaling lipids, which governs essential physiological processes underlying neuronal functions and overall cellular homeostasis and viability.[21–23]

Metabolism of S1P is a quite complex biological process involving a number of different highly specialized enzymes, and a fine

Received 8 April 2022; accepted 6 September 2022;
https://doi.org/10.1016/j.ymthe.2022.09.004.

[11]Present address: COMBINEDBrain, 1510 Old Hickory Blvd., Brentwood, TN 37027, USA

Correspondence: Vittorio Maglione, IRCCS Neuromed, Pozzilli (IS) 86077, Italy.
E-mail: vittorio.maglione@neuromed.it

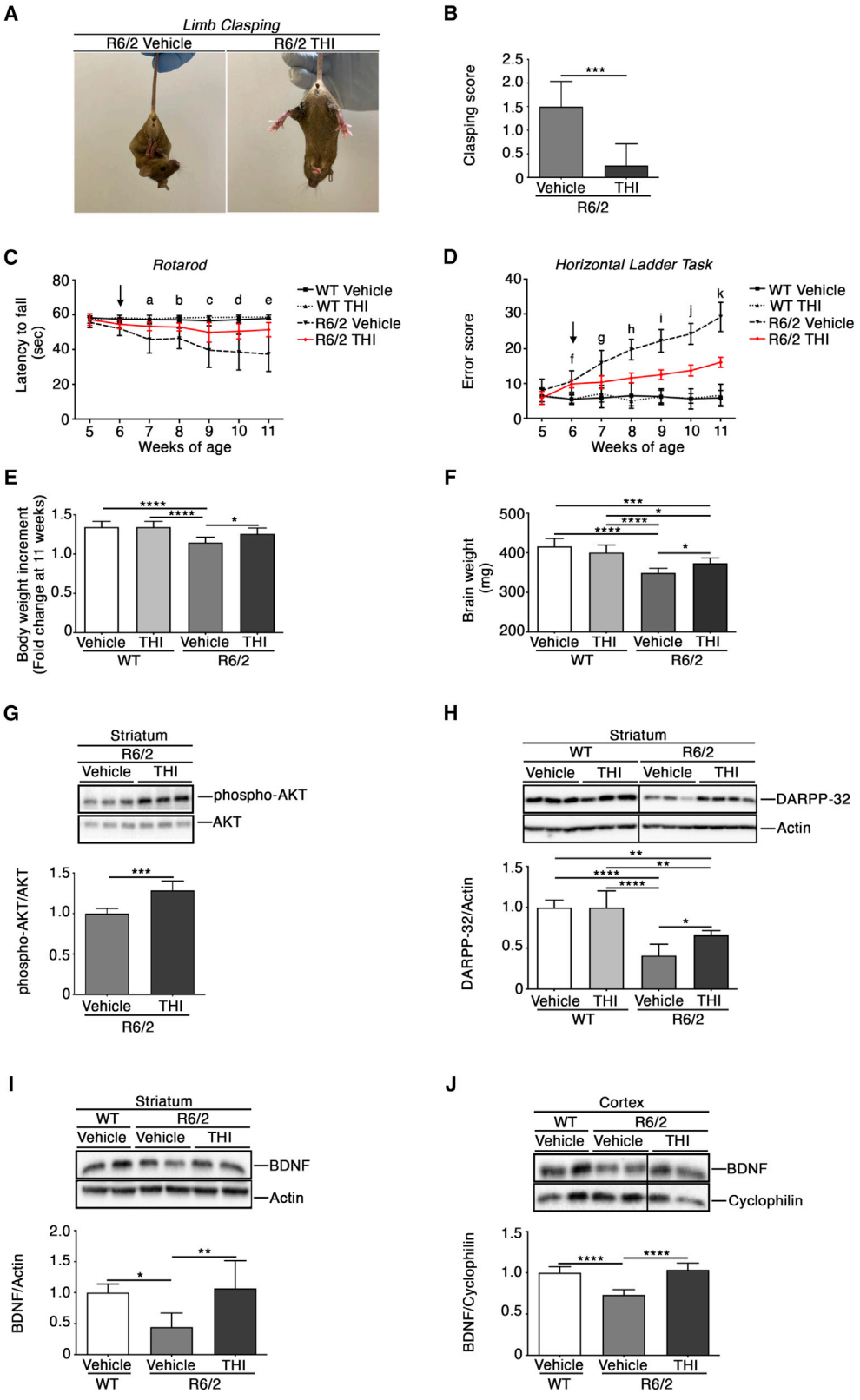

(legend on next page)

balance between synthesis and degradation is normally required for cellular homeostasis and functions. S1P is synthesized by sphingosine kinase-1 and -2 (SPHK1 and 2), and irreversibly degraded by S1P lyase (SGPL1).[24] Once synthesized, S1P may be transported outside the cells through the SPNS2 transporter and binds a family of five specific G protein-coupled receptors ($S1PR_{1-5}$).[21]

Reduced levels of SPHK1, and the concomitant increase in the levels of SGPL1, have been reported in different HD models as well as in human post-mortem brains from HD patients.[19] This imbalance may plausibly underlie the decremented bioavailability of S1P.[19]

The degradative enzyme SGPL1 represents a key regulator in the maintenance of balanced S1P levels and other sphingolipid intermediates that influence various aspects of cell growth, proliferation, and cell death.[25]

The role of SGPL1 in the nervous system is still debated and at times controversial.[26–29] While specific inactivation of SGPL1 in neurons induces S1P accumulation, by altering presynaptic functions[30] and autophagic flux,[31] full-body partial ablation of *Sgpl1* gene does not lead to any accumulation of S1P in brain tissues, and this is beneficial in a mouse model of experimental autoimmune encephalomyelitis.[32]

Inhibition of SGPL1, by 2-acetyl-5-tetrahydroxybutyl imidazole (THI),[33] reduced cell apoptosis in different *in vitro* HD models[19,34] and suppressed dystrophic muscle degeneration in experimental models of Duchenne muscle dystrophy.[35]

In this study, we report the therapeutic potential of THI in two different *in vivo* experimental models of HD.

THI normalized levels of brain-derived neurotrophic factor (BDNF) with associated neuroprotective effect preserved myelin integrity and stimulated synaptic functions in HD mice; it also normalized levels of glycosphingolipids (hexosylceramides), activated autophagy, and reduced Htt accumulation in the brain of HD mice.

Our findings reinforce the potential role of (glyco)sphingolipid pathways in HD pathogenesis, and further support their pharmacological targeting for the development of HD therapies.

RESULTS

Treatment with THI mitigates motor deficit and evokes the activation of pro-survival pathways in R6/2 mice

To test the hypothesis that inhibition of SGPL1 might be beneficial in *in vivo* models of HD, early manifest R6/2 mice (6 weeks old) and aged-matched wild-type (WT) littermates were daily intraperitoneally (i.p.) injected with 0.1 mg/kg THI, the lowest concentration reported to be safe *in vivo*,[36] or vehicle, and motor function was analyzed.

THI-treated HD mice did not exhibit the characteristic clasping behavior (Figures 1A and 1B) and performed significantly better than vehicle-treated controls during the whole period of the treatment as assessed by rotarod and horizontal ladder task (Figures 1C

Figure 1. Treatment with THI mitigates motor deficit and evokes the activation of pro-survival pathways in R6/2 mice

(A and B) Limb-clasping response of vehicle- and THI-treated R6/2 mice at age 11 weeks. (C) Motor performance assessed by rotarod in vehicle- and THI-treated WT and R6/2 mice. Values are represented as mean ± SD N = 8 (females N = 5; males N = 3) for each group of mice. Two-way ANOVA, (a) R6/2 vehicle versus WT vehicle ****p < 0.0001; R6/2 vehicle versus WT THI ****p < 0.0001; R6/2 vehicle versus R6/2 THI *p < 0.05; (b) R6/2 vehicle versus WT vehicle ***p < 0.001; R6/2 vehicle versus WT THI ****p < 0.0001; (c) R6/2 vehicle versus WT vehicle ****p < 0.0001; R6/2 vehicle versus WT THI ****p < 0.0001; R6/2 THI versus WT THI **p < 0.01; R6/2 vehicle versus R6/2 THI ***p < 0.001; (d) R6/2 vehicle versus WT vehicle ****p < 0.0001; R6/2 vehicle versus WT THI ****p < 0.0001; R6/2 THI versus WT THI *p < 0.05; R6/2 vehicle versus R6/2 THI ****p < 0.0001; (e) R6/2 vehicle versus WT vehicle ****p < 0.0001; R6/2 vehicle versus WT THI ****p < 0.0001; R6/2 THI versus WT THI *p < 0.05; R6/2 vehicle versus R6/2 THI ****p < 0.0001. (D) Motor performance assessed by Horizontal Ladder Task in vehicle- and THI-treated WT and R6/2 mice. The arrows indicate the treatment initiation. Values are represented as mean ± SD N = 8 (females N = 5; males N = 3) for each group of mice. Two-way ANOVA, (f) R6/2 vehicle versus WT vehicle **p < 0.01; R6/2 THI versus WT vehicle *p < 0.05; R6/2 vehicle versus WT THI **p < 0.01; R6/2 THI versus WT THI *p < 0.05; (g) R6/2 vehicle versus WT vehicle ****p < 0.0001; R6/2 THI versus WT vehicle *p < 0.05; R6/2 vehicle versus WT THI ****p < 0.0001; R6/2 vehicle versus R6/2 THI ***p < 0.001; (h) R6/2 vehicle versus WT vehicle ****p < 0.0001; R6/2 THI versus WT vehicle **p < 0.01; R6/2 vehicle versus WT THI ****p < 0.0001; R6/2 THI versus WT THI ****p < 0.0001; R6/2 vehicle versus R6/2 THI ****p < 0.0001; (i) R6/2 vehicle versus WT vehicle ****p < 0.0001; R6/2 THI versus WT vehicle ****p < 0.0001; R6/2 vehicle versus WT THI ****p < 0.0001; R6/2 THI versus WT THI ****p < 0.0001; R6/2 vehicle versus R6/2 THI ****p < 0.0001; (j) R6/2 vehicle versus WT vehicle ****p < 0.0001; R6/2 THI versus WT vehicle ****p < 0.0001; R6/2 vehicle versus WT THI ****p < 0.0001; R6/2 THI versus WT THI ****p < 0.0001; R6/2 vehicle versus R6/2 THI ****p < 0.0001; (k) R6/2 vehicle versus WT vehicle ****p < 0.0001; R6/2 THI versus WT vehicle ****p < 0.0001; R6/2 vehicle versus WT THI ****p < 0.0001; R6/2 THI versus WT THI ****p < 0.0001; R6/2 vehicle versus R6/2 THI ****p < 0.0001. (E) Fold of change of body weight loss in vehicle- and THI-treated WT and R6/2 mice at age 11 weeks. Values are represented as mean ± SD N = 8 (females N = 5; males N = 3) for each group of mice. Two-way ANOVA, *p < 0.05; ****p < 0.0001. (F) Brain weight of vehicle- and THI-treated WT and R6/2 mice. Values are represented as mean ± SD N = 8 (females N = 5; males N = 3) for each group of mice. Two-way ANOVA, *p < 0.05; ***p < 0.001; ****p < 0.0001. (G) Representative cropped immunoblotting and densitometric analysis of AKT kinase in striatal tissues from vehicle- and THI-treated R6/2 mice at age 11 weeks. Values are represented as mean ± SD. N = 6 (females N = 3; males N = 3) for each group of mice. Unpaired t test, ***p < 0.001. (H) Representative cropped immunoblotting and densitometric analysis of DARPP-32 in striatal tissues from vehicle- and THI-treated WT and vehicle- and THI-treated R6/2 mice at age 11 weeks. Values are represented as mean ± SD. N = 5 (females N = 3; males N = 2) for both vehicle- and THI-treated WT mice. N = 6 (females N = 3; males N = 3) for both vehicle and THI-treated R6/2 mice. Two-way ANOVA, *p < 0.05; **p < 0.01; ****p < 0.0001. (I) Representative cropped immunoblotting and densitometric of BDNF in striatal tissues from vehicle-treated WT and vehicle- and THI-treated R6/2 mice at age 11 weeks. Non-adjacent samples were separated by a black line. Values are represented as mean ± SD. N = 6 (females N = 3; males N = 3) for each group of mice. One-way ANOVA, *p < 0.05; **p < 0.01. (J) Representative cropped immunoblotting and densitometric analysis of BDNF in cortical tissues from vehicle-treated WT and vehicle- and THI-treated R6/2 mice at age 11 weeks. In each immunoblotting, all samples were run on the same gel. Non-adjacent samples were separated by a black line. Values are represented as mean ± SD. N = 6 (females N = 3; males N = 3) for each group of mice. One-way ANOVA, ****p < 0.0001.

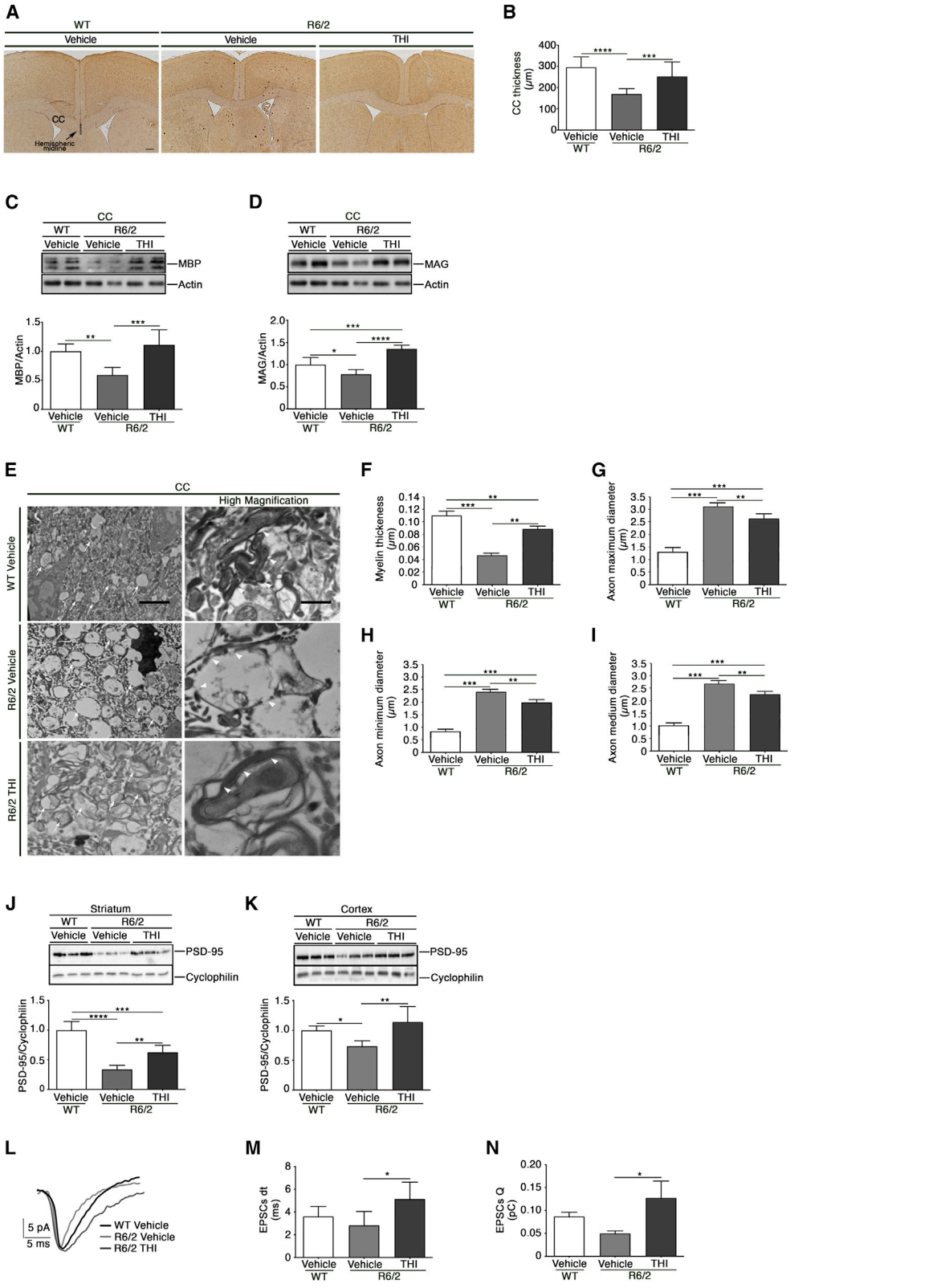

(legend on next page)

and 1D). Also, both brain and body weight loss were attenuated by THI administration (Figures 1E and 1F). No evidence of adverse events was observed in WT animals.

Next, we explored the potential neuroprotective effects of THI in R6/2 mouse brain.

Administration of the compound was associated with increased phosphorylation of the pro-survival kinase AKT (Figure 1G) and with increased protein expression of striatal dopamine- and cAMP-regulated protein 32 (DARPP-32) (Figure 1H), a specific marker of medium spiny neurons,[37] whose downregulation classically correlates with neurodegeneration in HD.[38]

Importantly, THI administration preserved normal levels of BDNF in both striatum and cortex of R6/2 mice (Figures 1I and 1J). No changes in WT animals were observed (Figures S1A–S1C).

THI treatment preserves white matter integrity and ameliorates synaptic activity in HD cortical pyramidal neurons

Alterations in the corpus callosum (CC) and white matter integrity have been reported early in the disease in both HD animal models and human patients.[9,39–42]

Semiquantitative analysis of anatomical structure of the CC revealed that chronic infusion of THI prevented the reduction of its thickness[43] in R6/2 mice (Figures 2A and 2B).

Changes in the CC of THI-treated R6/2 mice were associated with preservation of normal levels of the myelin markers, myelin basic protein (MBP) and myelin-associated glycoprotein (MAG) (Figures 2C and 2D).

The beneficial effect of the treatment was confirmed by electron microscopy, which revealed the presence of giant axons with abnormal myelin sheaths and negligible axoplasm electron density in R6/2 mice (Figure 2E). Treatment with THI increased myelin thickness (Figure 2F) and reduced maximum, minimum, and medium axonal diameter in HD (Figures 2G–2I).

Further proofs of the ability of the compound to preserve axonal homeostasis and neuronal functions in HD mice came from both molecular and electrophysiological studies.

Treatment with THI preserved normal levels of post-synaptic density 95 protein (PSD-95) in both striatum and cortex of HD mice (Figures 2J and 2K).

PSD-95, a major constituent of glutamatergic excitatory synapses, is specifically enriched at the PSD and can regulate the alpha-amino-3-hydroxy-5-methyl-4-isoxazole propionic acid and N-methyl-D-aspartic acid receptor expression and activity in spines.[44,45]

In light of that, we recorded spontaneous excitatory post-synaptic currents (EPSCs) from L5 pyramidal neurons in temporal slices of WT and R6/2 mice.

Treatment with THI significantly increased both EPSC decay time and EPSC charge, carried by a single synaptic event in HD neurons

Figure 2. THI treatment preserves white matter integrity and ameliorates synaptic activity in HD cortical pyramidal neurons

(A) Representative micrograph of CC thickness of vehicle-treated WT (left), vehicle- (center) and THI-treated R6/2 (right) mice at age 11 weeks. Scale bar, 100 μm. (B) Semiquantitative measurement of CC thickness (μm) in correspondence of the middle line of the brain as indicated in (A). Values are represented as mean ± SD. N = 4 (females N = 2; males N = 2) for each group of mice. One-way ANOVA, ***p < 0.001; ****p < 0.0001. (C) Representative cropped immunoblotting and densitometric analysis of MBP in CC protein lysate from vehicle-treated WT and vehicle- and THI-treated R6/2 mice at age 11 weeks. Values are represented as mean ± SD. N = 6 (females N = 3; males N = 3) for each group of mice. One-way ANOVA, **p < 0.01; ***p < 0.001. (D) Representative cropped immunoblotting and densitometric analysis of MAG in CC protein lysate from vehicle-treated WT and vehicle- and THI-treated R6/2 mice at age 11 weeks. Values are represented as mean ± SD. N = 6 (females N = 3; males N = 3) for each group of mice. One-way ANOVA, *p < 0.05; ***p < 0.001; ****p < 0.0001. Both MBP and MAG panels derived from the same gel. The same actin blot appears twice. (E) Representative electron micrographs of axons in the CC from vehicle-treated WT and vehicle- and THI-treated R6/2 mice at age 11 weeks. Giant axons (left panels) are indicated by arrows. Myelin sheet abnormities (right panels) are indicated by arrowheads. Scale bars, 1 μm (left panels) and 0.2 μm (right panels; high magnification). (F) Bar graphs representing the myelin thickness in the CC from vehicle-treated WT and vehicle- and THI-treated R6/2 mice at age 11 weeks. Values are represented as mean ± SEM. N = 4 (females N = 2; males N = 2) for each group of mice. Fifty axons for each experimental group. One-way ANOVA, **p < 0.01; ***p < 0.001. (G) Bar graphs representing the axon maximum diameter in the CC from vehicle-treated WT and vehicle- and THI-treated R6/2 mice at age 11 weeks. Values are represented as mean ± SEM. N = 4 (females N = 2; males N = 2) for each group of mice. Fifty axons for each experimental group were counted. One-way ANOVA, **p < 0.01; ***p < 0.001. (H) Bar graphs representing the axon minimum diameter in the CC from vehicle-treated WT and vehicle- and THI-treated R6/2 mice at age 11 weeks. Values are represented as mean ± SEM. N = 4 (females N = 2; males N = 2) for each group of mice. Fifty axons for each experimental group were counted. One-way ANOVA, **p < 0.01; ***p < 0.001. (I) Bar graphs representing the axon mean diameter in the CC from vehicle-treated WT and vehicle- and THI-treated R6/2 mice at age 11 weeks. Values are represented as mean ± SEM. N = 4 (females N = 2; males N = 2) for each group of mice. Fifty axons for each experimental group were counted. One-way ANOVA, **p < 0.01; ***p < 0.001. (J) Representative cropped immunoblotting and densitometric analysis of PSD-95 in protein lysates from striatum of vehicle-treated WT and vehicle- and THI-treated R6/2 mice at age 11 weeks. Values are represented as mean ± SD. N = 6 (females N = 3; males N = 3) for each group of mice. One-way ANOVA, **p < 0.01; ***p < 0.001; ****p < 0.0001. (K) Representative cropped immunoblotting and densitometric analysis of PSD-95 in the protein lysates from cortex of vehicle-treated WT and vehicle- and THI-treated R6/2 mice at age 11 weeks. Values are represented as mean ± SD. N = 6 (females N = 3; males N = 3) for each group of mice. One-way ANOVA, *p < 0.05; **p < 0.01. (L) Typical EPSC traces recorded from, respectively, vehicle-treated WT (black), and vehicle- (light gray) and THI-Treated R6/2 mice (dark gray) at age 8 weeks. (M) Bar graphs representing mean of EPSC decay time$_{90\text{-}10}$ obtained from five, five, and six cells from vehicle-treated WT, vehicle- and THI-Treated R6/2 mice, respectively. One-way ANOVA, *p < 0.05. (N) Bar graphs representing EPSC mean of charge obtained from five, four, and six cells from WT, R6/2 untreated, and R6/2 treated mice, respectively. One-way ANOVA, *p < 0.05.

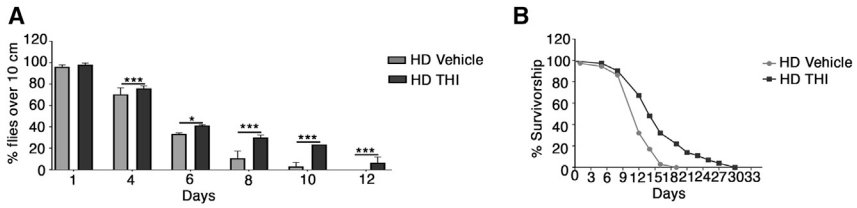

C

	Mean Lifespan (day)	Mean Lifespan Change (%)	Maximun Lifespan (day)	Maximum Lifespan Change (%)
HD Vehicle	12.34 ± 0.1	-	15 ± 0.1	-
HD THI	16.04 ± 0.08**	29.98	23 ± 0.08**	53.33

Figure 3. THI ameliorates locomotor function and increases lifespan in a *Drosophila melanogaster* HD model

(A) Analysis of locomotor functions in untreated versus THI-treated HD *D. melanogaster* HD model after 12 days of treatment, as assessed by Climbing test. Values are represented as mean ± SD. Unpaired t test, *p < 0.05; ***p < 0.001. (B) Comparison of age-dependent survival curves in untreated and THI-treated HD flies. Mantel-Cox test, p < 0.0001. (C) Percentage of medium and maximum lifespan change. Values are represented as mean ± SD. Unpaired t test, **p < 0.01.

(Figures 2L–2N). No changes were observed in EPSC frequency, amplitude, and rise time (Figures S2A–S2C).

THI ameliorates locomotor function and increases lifespan in a *Drosophila Melanogaster* HD model

HD flies (genotype: elav-Gal4/+; UAS-HttFL-Q128/+), expressing human Htt cDNA encoding for full-length mHtt protein (Q128HD-FL), are characterized by a progressive age-dependent motor dysfunction and coordination difficulties.[46,47]

To assess any potential effect of THI on both lifespan and locomotor functions, Q128HD-FL transgenic flies were fed with either 50 μM THI-supplemented assay fly food (AF) medium or a control diet, with the AF medium as control.

Dietary THI significantly improved locomotor performance, as assessed by negative geotaxis assay (Figure 3A), and significantly extended lifespan in HD flies (Figures 3B and 3C).

THI treatment modulates the expression of sphingolipid-metabolizing enzymes and restores normal levels of hexosylceramides in HD mice

Treatment with THI may increase levels of S1P in both brain and peripheral organs.[48–50]

LC-MS/MS lipidomic analysis has shown no changes in the levels of S1P, sphingosine (Sph) and ceramides (Cer) neither in the striatal (Figures 4A–4C) nor in the cortical (Figures S3A–S3C) tissues from HD mice. Conversely, while no changes were observed for S1P, levels of sphingosine and of some ceramide species were significantly increased in brain tissues of WT mice (Figures S3D–S3I).

Nevertheless, qPCR analysis revealed that THI preserved normal expression of ceramide synthases *CerS1* and *CerS2* (Figures 4D and 4E) and serine palmitoyltransferase long-chain base subunit 1 *Sptlc1* (Figure 4F), one of the enzymes involved in the *de novo* synthesis of sphingolipids, described previously as reduced in the striatum of HD mice.[18] Interestingly, the treatment increased expression of S1P transporter Spns2 (Figure 4G), and associated with the incremented levels of $S1PR_1$ and $S1PR_5$ proteins (Figures 4H and 4I).

Importantly, as reported in Figure 4J, analysis of the striatum revealed that THI restored normal levels of hexosylceramides (HexCer) C18:0 and C24:1 in HD mice. Conversely, no changes were observed for HexCer C16:0 and C18:1.

Analysis of the cortex, similarly to the striatum, showed that THI restored normal levels of HexCer C18:0 (Figure S3J). However, no effects were observed for HexCer C16:0, C18:1, and 24:1 (Figure S2L). WT animals did not display any variation in the striatum (Figure S3K) or in the cortex (Figure S3L).

Since the lipidomic analysis did not clarify whether the increase in hexosylceramides was attributable to glucosylceramide (GluCer), galactosylceramide (GalCer), or to both, we performed a semiquantitative analysis for assessing levels of GluCer in mouse brain tissues.

Immunoblotting (slot blotting) analysis by using a specific antibody against GluCer[51] showed increased levels of GluCer in striatal tissues of R6/2 mice compared with WT littermates (Figure S3M).

Finally, to establish whether GluCer accumulation was due to any change in the expression of its metabolizing enzymes, we assessed the expression of GluCer synthase (*Ugcg*) and glucocerebrosidase beta 1 and 2 enzymes (*Gba1/2*), classically involved in the GluCer degradation.[52]

Treatment with THI restored normal mRNA levels of *Ugcg* (Figure 4K) and significantly increased the expression of *Gba1* (Figure 4L) in the striatum of HD mice compared with WT littermates. No changes in *Gba2* were observed (Figure 4M).

Defects in HexCer metabolism are detectable early in the disease course in different HD mouse models

To possibly clarify whether the accumulation of hexosylceramides might occur early in the disease, we assessed their levels in

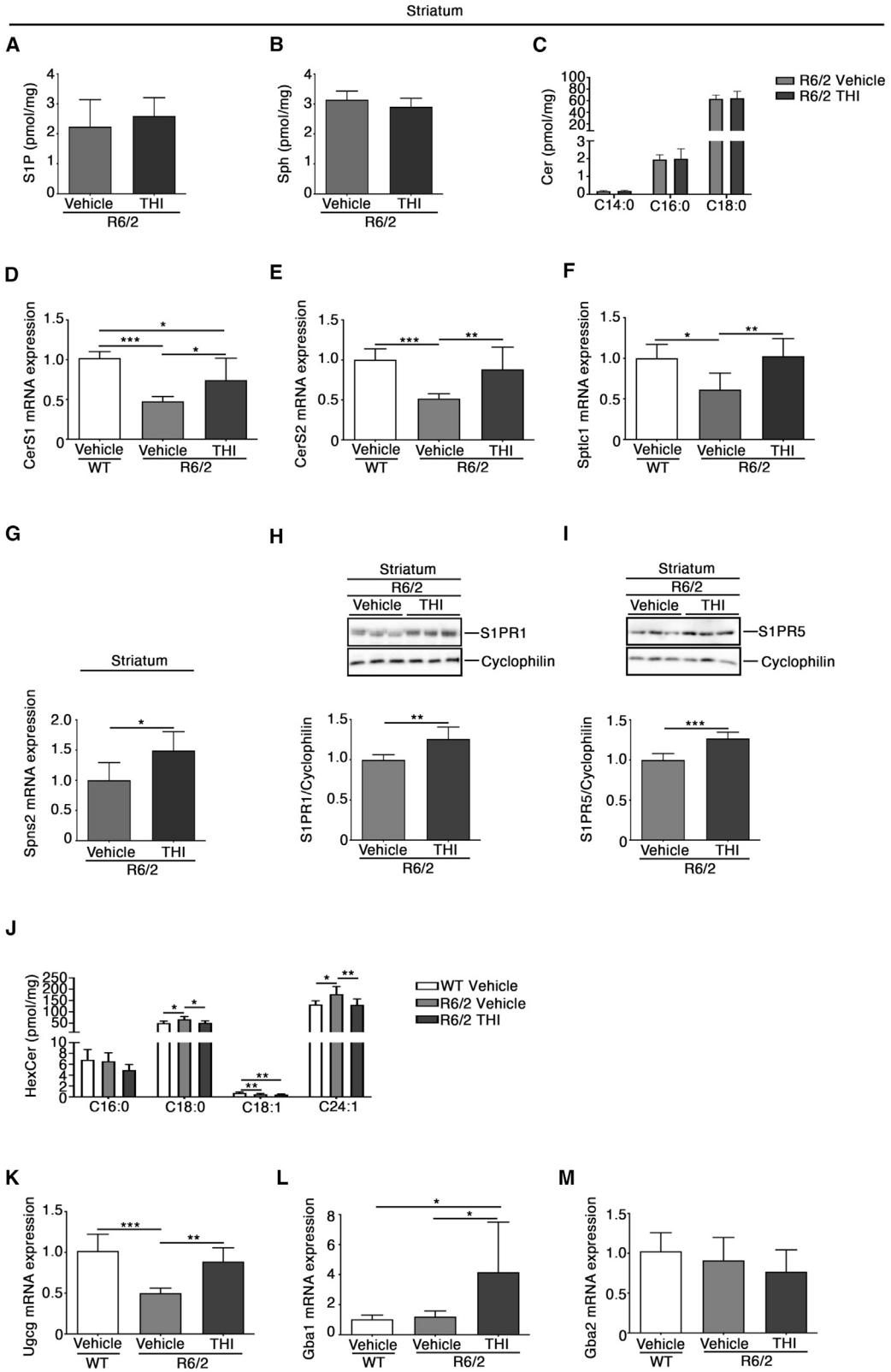

(legend on next page)

pre-manifest (4-week-old) R6/2 mice and age-matched WT littermates.

As reported in Figure 5A, mass spectrometry analysis revealed that HexCer C24:1 was already increased in the striatum of 4-week-old HD mice. No difference was observed in the cortex (Figure S4A).

Next, we assessed whether such an increase was associated with any defect in the transcription of GluCer-metabolizing enzymes. qPCR analysis revealed no difference in the expression profile of *Ugcg*, *Gba1*, and *Gba2* transcripts (Figures 5B–5D).

Finally, to establish whether these defects were shared by other HD mouse models, we carried out a semiquantitative analysis of GluCer in both striatal and cortical tissues from early manifest heterozygous zQ175 (20-week-old) and transgenic YAC128 (13-week-old) HD mice.

Slot blot analysis showed a significant increase in GluCer content in the cortical lysates of both HD mouse models with respect to the WT littermates (Figures 5E and 5F), whereas no changes were observed in the striatum (Figures S4B and S4C).

Both deficiency of wtHtt and overexpression of mutant exon-1 fragments increase GluCer levels *in vitro*

To clarify the potential role of Htt in the (dys)regulation of the GluCer metabolism, we determined the GluCer content and investigated the gene expression profile of metabolizing enzymes in mouse immortalized striatal-derived cell lines, expressing endogenous levels of either WT ($STHdh^{7/7}$) or mutant ($STHdh^{111/111}$) Htt.

$STHdh^{111/111}$ cells displayed increased levels of GluCer when compared with $STHdh^{7/7}$ (Figure 6A). The accumulation of GluCer was associated with reduced *Ugcg* and increased *Gba1* mRNA levels (Figures 6B and 6C). No statistically significant changes were observed in *Gba2* mRNA expression (Figure 6D).

Next, we investigated whether Htt might regulate GluCer pathways. $STHdh^{7/7}$ cells were, therefore, transiently transfected with either control or Htt siRNAs. Forty-eight hours after transfections, the reduction of wtHtt (Figure 6E) was associated with increased levels of GluCer (Figure 6F) with no influence on *Ugcg* or *Gba1/2* gene expression (Figures 6G–6I).

Finally, we explored any possible effect of ectopic expression of mHtt exon-1 fragments might have in WT cells.

$STHdh^{7/7}$ were transiently transfected with the EGFP-mHtt exon-1 fragment-expressing plasmid. Similar to that observed in the wtHtt lowering experiments, overexpression of mHtt fragments correlated with a significant increase of GluCer levels (Figures 6J and 6K), suggesting that mHtt might affect the function of the wtHtt protein by reducing its bioavailability.

THI treatment modulates the expression of vesicle trafficking/autophagic markers and reduces Htt aggregation

Based on the association between (glyco)sphingolipids and intracellular trafficking as well as the endomembrane system,[53–55] we investigated the potential effect of THI on the expression of endomembrane markers in the striatum of R6/2 mice.

As reported in Figures 7A and 7B, THI reduced the expression of the *trans*-Golgi network marker, TGN38, with no effect on the *cis* marker GM130. Moreover, the treatment significantly increased the expression of LAMP2 (lysosome-associated membrane glycoprotein 2) (Figure 7C), which usually maintains lysosomal stability and participates in the autophagic pathway.[56,57]

Figure 4. THI treatment modulates the expression of sphingolipid-metabolizing enzymes and restores normal levels of hexosylceramides in HD mice

(A) Lipidomic analysis by LC-MS/MS of S1P in striatal tissues of vehicle- and THI-treated R6/2 mice at age 11 weeks. Values are represented as mean ± SD. N = 7 (females N = 4; males N = 3) for each group of mice. (B) Lipidomic analysis by LC-MS/MS of Sph in striatal tissues of vehicle- and THI-treated R6/2 mice at age 11 weeks. Values are represented as mean ± SD. N = 7 (females N = 4; males N = 3) for each group of mice. (C) Lipidomic analysis by LC-MS/MS of Cer in striatal tissues of vehicle- and THI-treated R6/2 mice at age 11 weeks. Values are represented as mean ± SD. N = 7 (females N = 4; males N = 3) for each group of mice. (D) qPCR analysis of *CerS1* in the striatum of vehicle-treated WT and vehicle- and THI-treated R6/2 mice at age 11 weeks. Values are represented as mean ± SD. N = 6 (females N = 3; males N = 3) for each group of mice. One-way ANOVA, *$p < 0.05$; ***$p < 0.001$. (E) qPCR analysis of *CerS2* in the striatum of vehicle-treated WT and vehicle- and THI-treated R6/2 mice at age 11 weeks. Values are represented as mean ± SD. N = 6 (females N = 3; males N = 3) for each group of mice. One-way ANOVA, **$p < 0.01$; ***$p < 0.001$. (F) qPCR analysis of *Sptlc1* in the striatum of vehicle-treated WT and vehicle- and THI-treated R6/2 mice at age 11 weeks. Values are represented as mean ± SD. N = 6 (females N = 3; males N = 3) for each group of mice. One-way ANOVA, *$p < 0.05$; **$p < 0.01$. (G) qPCR analysis of *Spns2* in the striatum of vehicle- and THI-treated R6/2 mice at age 11 weeks. Values are represented as mean ± SD. N = 5 (females N = 3; males N = 2) for each group of mice. Unpaired t test, *$p < 0.05$. (H) Representative cropped immunoblotting and densitometric analysis of $S1PR_1$ in the protein lysates from striatum of vehicle- and THI-treated R6/2 mice at age 11 weeks. Values are represented as mean ± SD. N = 6 (females N = 3; males N = 3) for each group of mice. Unpaired t test, **$p < 0.01$. (I) Representative cropped immunoblotting and densitometric analysis of $S1PR_5$ in the protein lysates from striatum of vehicle- and THI-treated R6/2 mice at age 11 weeks. Values are represented as mean ± SD. N = 6 (females N = 3; males N = 3) for each group of mice. Unpaired t test, ***$p < 0.001$. (J) Lipidomic analysis by LC-MS/MS of HexCer 16:0, 18:0, 18:1, and 24:1 in striatal tissues of vehicle-treated WT and vehicle- and THI-treated R6/2 mice at age 11weeks . Values are represented as mean ± SD. N = 7 (females N = 4; males N = 3) for each group of mice. One-way ANOVA, *$p < 0.05$; **$p < 0.01$. (K) qPCR analysis of *Ugcg* in the striatum of vehicle-treated WT and vehicle- and THI-treated R6/2 mice at age 11 weeks. Values are represented as mean ± SD. N = 6 (females N = 3; males N = 3) for each group of mice. One-way ANOVA, **$p < 0.01$; ***$p < 0.001$. (L) qPCR analysis of *Gba1* in the striatum of vehicle-treated WT and vehicle- and THI-treated R6/2 mice at age 11 weeks. Values are represented as mean ± SD. N = 6 (females N = 3; males N = 3) for each group of mice. One-way ANOVA, *$p < 0.05$. (M) qPCR analysis of *Gba2* in the striatum of vehicle-treated WT and vehicle- and THI-treated R6/2 mice at age 11 weeks. Values are represented as mean ± SD. N = 6 (females N = 3; males N = 3) for each group of mice.

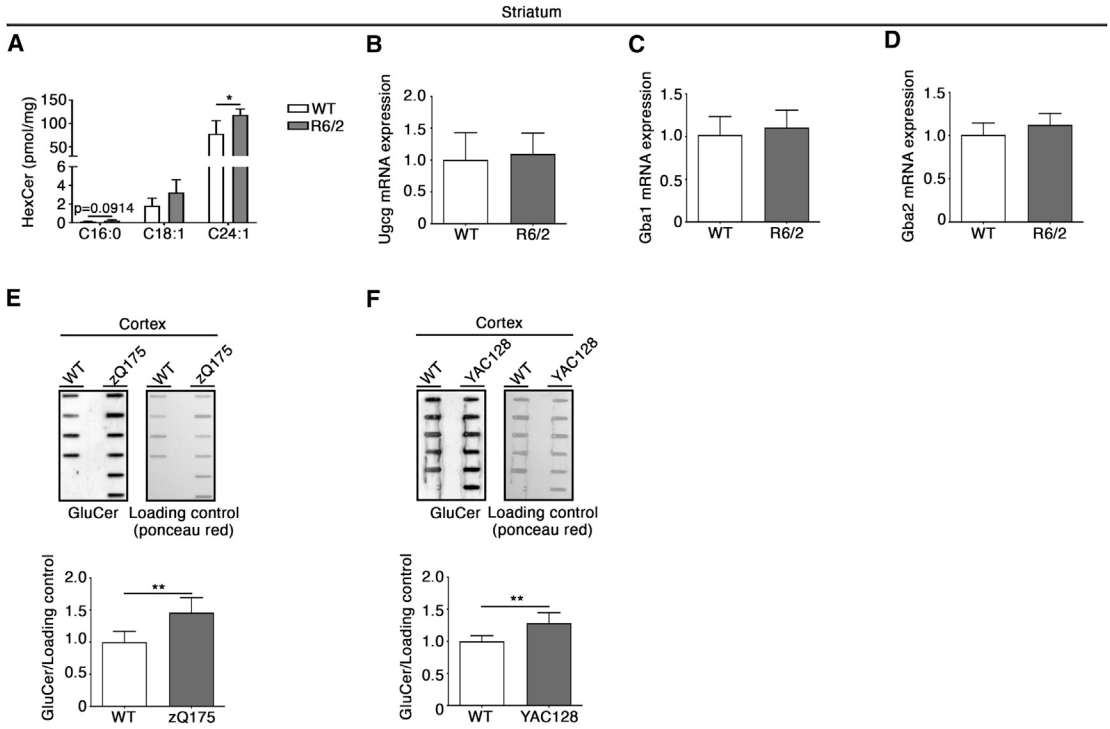

Figure 5. Defects in HexCer metabolism are detectable early in the disease course in different HD mouse models

(A) Lipidomic analysis by LC-MS/MS of HexCer 16:0, 18:0, and 24:1 in striatal tissues of pre-manifest (4-week-old) R6/2 mice and aged-matched WT littermates. Values are represented as mean ± SD. N = 4 males for each group of mice. Unpaired t test, *p < 0.05. (B) qPCR analysis of *Ugcg* in striatal tissues of pre-manifest (4-week-old) R6/2 mice and aged-matched WT littermates. Values are represented as mean ± SD. N = 6 (females N = 3; males N = 3) for each group of mice. (C) qPCR analysis of *Gba1* in striatal tissues of pre-manifest (4-week-old) R6/2 mice and aged-matched WT littermates. Values are represented as mean ± SD. N = 6 (females N = 3; males N = 3) for each group of mice. (D) qPCR analysis of *Gba2* in striatal tissues of pre-manifest (4-week-old) R6/2 mice and aged-matched WT littermates. Values are represented as mean ± SD. N = 6 (females N = 3; males N = 3) for each group of mice. (E) Slot blotting and densitometric analysis of GluCer in cortical tissues from WT and heterozygous zQ175 mice at age 20 weeks. Values are represented as mean ± SD. N = 4 for WT (females N = 3; males N = 1) mice; N = 6 (females N = 3; males N = 3) for HD mice. Ponceau red was used as total protein loading control. Unpaired t test, **p < 0.01. (F) Slot blotting and densitometric analysis of GluCer in cortical tissues from WT and YAC128 mice at age 13 weeks. Values are represented as mean ± SD. N = 5 for WT (females N = 3; males N = 2) mice; N = 6 (females N = 3; males N = 3) for HD mice. Ponceau red was used as total protein loading control. Unpaired t test, **p < 0.01.

THI-mediated stimulation of the autophagic flux was confirmed by the modulation of the expression of LC3 and Beclin1 (Figures 7D and 7E), two specific markers of autophagy.[58] No changes in any of these markers were observed in WT animals (Figures S5A–S5F).

Stimulation of lysosomal/autophagic machinery has already been associated with reduction of mHtt aggregation,[59] a typical hallmark of HD.[60] We therefore explored whether THI might have any effect on protein aggregation.

Immunohistochemical analysis revealed that treatment with THI reduced the number of mHtt EM48-positive nuclear inclusions in the striatum of R6/2 mice (Figures 7F and 7G).

This result was further confirmed by immunoblotting analysis in which EM48-positive SDS-insoluble mHtt aggregates were barely detectable in HD striatal protein lysates (Figure 7H) after THI treatment.

Previous evidence indicates that mHtt aggregates may also contain wtHtt.[61–67] Coherently, in this study, we report nuclear inclusions of wtHtt in R6/2 mice brain tissues (Figure 7I). To better understand whether the presence of the two species of Htt might be the result of any existing interaction, immunoprecipitation studies were carried out.

After mHtt immunoprecipitation using the EM48 antibody, immunoblotting analysis with the mab2166 antibody, which recognizes a protein epitope absent in the mHtt exon-1 fragments,[68–70] highlighted the presence of wtHtt in the stacking part of the gel, where mHtt aggregates classically are trapped (Figures 7K and 7L).

Administration of THI reduced mHtt aggregation and, interestingly, also diminished the number of wtHtt nuclear inclusions (Figure 7J), which contextually resulted in a detectable increased expression of soluble full-length wtHtt (Figures 7K and 7L) in the striatal tissues of HD mice. This result suggested a potential augmented bioavailability of "free" wt protein after THI.

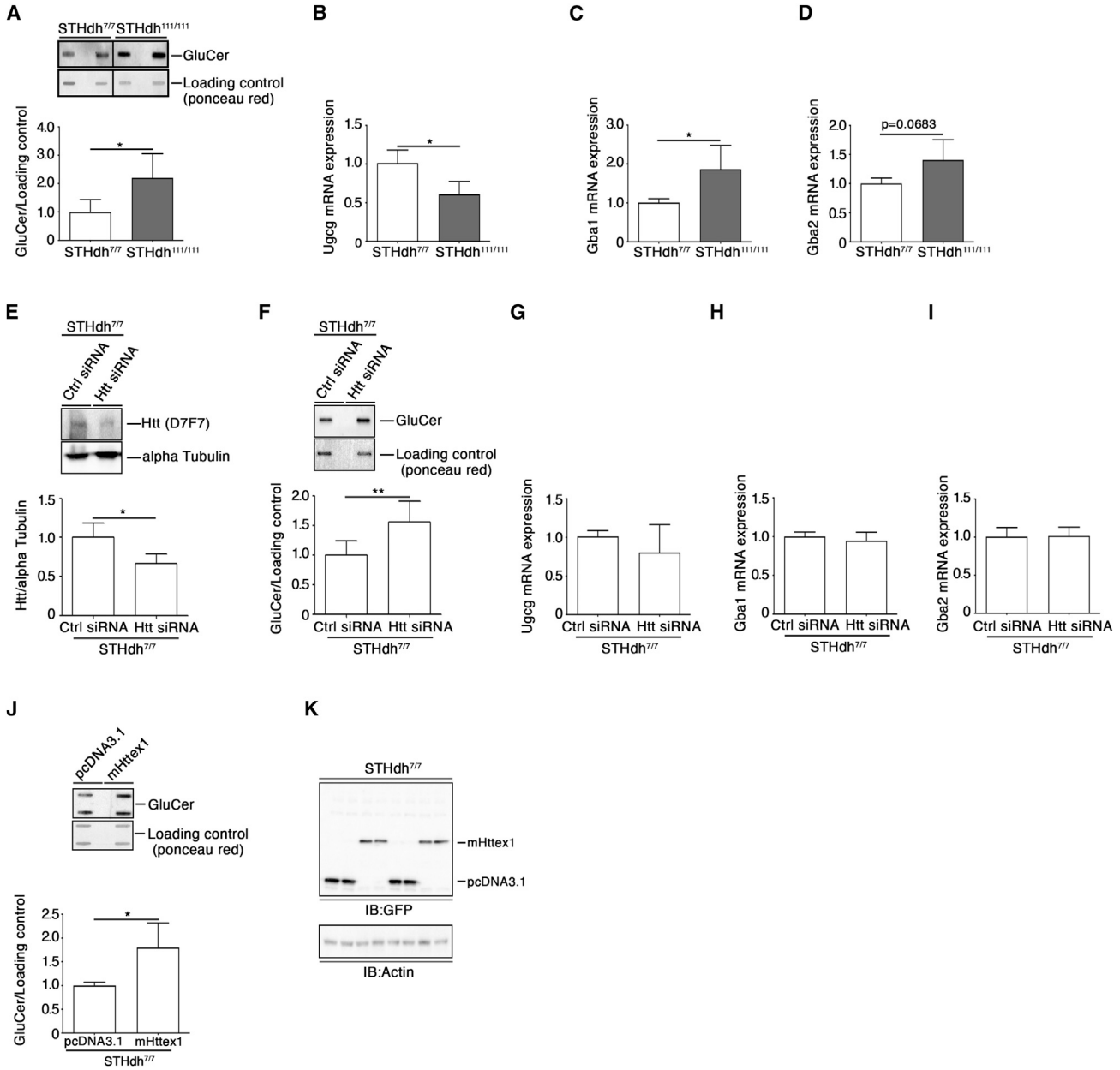

Figure 6. Both deficiency of wtHtt and overexpression of mutant exon-1 fragments increase GluCer levels *in vitro*

(A) Representative cropped slot blotting and densitometric analysis of GluCer in WT (STHdh$^{7/7}$) and HD (STHdh$^{111/111}$) total protein lysate. Values are represented as mean ± SD of four independent experiments. Ponceau red was used as total protein loading control. Unpaired t test, *p < 0.05. (B) qPCR analysis of *Ugcg* in STHdh$^{7/7}$ and STHdh$^{111/111}$ cells. Values are represented as mean ± SD of four independent experiments. Unpaired t test, *p < 0.05. (C) qPCR analysis of *Gba1* in STHdh$^{7/7}$ and STHdh$^{111/111}$ cells. Values are represented as mean ± SD of four independent experiments. Unpaired t test, *p < 0.05. (D) qPCR analysis of *Gba2* in STHdh$^{7/7}$ and STHdh$^{111/111}$ cells. Values are represented as mean ± SD of four independent experiments. (E) Representative cropped immunoblotting and densitometric analysis of wtHtt in STHdh$^{7/7}$ after 48 h of transfection with either control (CTRL) or Htt (HTT) small interfering RNA (siRNA). Values are represented as mean ± SD of four independent experiments. Unpaired t test, *p < 0.05. (F) Representative cropped slot blotting and densitometric analysis of GluCer in STHdh$^{7/7}$ cells after 48 h of transfection with either control (CTRL) or Htt (HTT) small interfering RNA (siRNA). Values are represented as mean ± SD of four independent experiments. Ponceau red was used as total protein loading control. Unpaired t test, **p < 0.01. (G) qPCR analysis of *Ugcg* in STHdh$^{7/7}$ cells after 48 h of transfection with either control (CTRL) or Htt (HTT) small interfering RNA (siRNA). Values are represented as mean ± SD of four independent experiments. (H) qPCR analysis of *Gba1* in STHdh$^{7/7}$ cells after 48 h of transfection with either control (CTRL) or Htt (HTT) small interfering RNA (siRNA). Values are represented as mean ± SD of four independent experiments. (I) qPCR analysis of *Gba2* in STHdh$^{7/7}$ cells after

(legend continued on next page)

DISCUSSION

In this study, we demonstrated that chronic infusion of THI, an inhibitor of the S1P degradative enzyme, SGPL1, was shown to be therapeutically effective in two experimental models of HD.

Importantly, we reported, for the first time, that Htt protein plays a key role in the regulation of levels of some glycosphingolipid species.

The ability of THI to evoke not only the activation of the neuroprotective kinase AKT and the increase of DARPP-32 expression but also to counteract either BDNF reduction or abnormal increase of mHtt aggregates, classical hallmarks of the disease,[60] highlighted the disease-modifying properties of the compound. In line with that, THI administration was found also to preserve white matter integrity and to ameliorate synaptic activity.

Cumulatively, these findings suggest a therapeutic action of THI *in vivo*. The beneficial effects were also observed in a *D. melanogaster* HD model.

Administration of THI resulted in the regulation of different molecular events, including the modulation of (glyco)sphingolipid pathways with no change in the levels of S1P. The reasons why we failed to detect any variation in S1P content in brain tissues by LC-MS/MS analysis may be multiple.

Evidence indicates that full-body SGPL1-deficient mice show increased levels of S1P in several tissues except the brain[32] and suggests that this enzyme may not be the only key regulator of S1P levels in the brain as in other tissues.[32] Moreover, due to the interconnectivity of the sphingolipid metabolism, other enzymes may modulate this interconversion and contribute to the maintenance of their levels.

Moreover, other aspects may be considered. Recently it has been reported that i.p. injection of the 3 mg/kg THI, for 1 week, was able to increase levels of S1P in the brain of streptozotocin-diabetic rats.[48] Here, we used the lowest concentration (0.1 mg/kg) of the inhibitor reported to be safe *in vivo*.[36] Thus, we can also speculate that, due to our experimental conditions (duration of treatment and concentration of the compound), any small and eventually "transient" variation of sphingolipids, such as sphingosine and S1P, induced by THI, may be not easily detectable in brain tissues. Nevertheless, the increased expression of both $S1PR_1$ and $S1PR_5$ and Spns2 indicates that the compound is able to stimulate the S1P axis, and it is suggestive of a possible change of S1P bioavailability, as occurs in other disease conditions.[71–74] Moreover, the evidence that THI normalized the expression of the enzymes involved in the synthesis of sphingolipids, including the *de novo* pathways, further highlighted the ability of the compound to modulate sphingolipid metabolic routes in the brain.

Finally, although not investigated in this study, we cannot exclude the possibility that THI may exert some additional beneficial effects on peripheral tissues, which may eventually contribute to the amelioration of the disease phenotype. In this context, the attenuation of the body weight loss that we observed could be likely due to a modulation of S1P pathways in the intestine, as already reported in our previous studies.[75]

Indeed, the treatment restored normal levels of hexosylceramide, which were found to be increased in both *in vitro* and *in vivo* experimental models.

Although, we cannot establish whether both GluCer and GalCer levels were increased in R6/2 mice, by mass spectrometry, the semi-quantitative analysis, performed in both *in vitro* and *in vivo*, suggested that HD models are characterized by an accumulation of GluCer, as recently reported in HD human postmortem brains.[12]

Accumulation of GluCer occurs in other neurodegenerative disorders[76,77] and it is usually attributable to either the deficient activity of lysosomal GBA1 or to the upregulation of UGCG.[78–80]

In this study, while we did not specifically measure any enzymatic activity, we demonstrated that accumulation of GluCer was associated with a reduced expression of *Ugcg* only in manifest R6/2 mice.

Although pre-manifest R6/2 mice displayed accumulation of HexCer, no defective gene expression was observed early in the disease. This result suggests that the alteration, detected at symptomatic stages of the disease, may be secondary to the glycolipid accumulation. Thus, it is plausible that the accumulation of GluCer may not be a mere consequence of the progression of the neurodegenerative processes, but rather it could represent a factor contributing to the pathogenesis of HD.

Our findings suggest that wtHtt may have a critical role in the regulation of GluCer levels. This is supported by the evidence that either the overexpression of mHtt-exon1 fragments or the loss of function of wtHtt exert similar effects in increasing GluCer levels, suggesting that mutant fragments may interfere with the normal function of the wt protein, through a possible "dominant negative" action.[63]

A number of studies indicates that mHtt inclusions can trap normal-length polyglutamine-containing proteins, including wtHtt, and affect their functions.[61–67] Our findings are in line with this concept and similarly to the mutant protein, wtHtt was found accumulated in the nuclei of striatal cells in R6/2 mice.

THI, by modulating sphingolipid metabolism, stimulates autophagic and lysosomal machinery and this in turn may promote the

48 h of transfection with either control (CTRL) or Htt (HTT) small interfering RNA (siRNA). Values are represented as mean ± SD of four independent experiments. (J) Representative cropped immunoblotting and densitometric analysis of GluCer in $STHdh^{7/7}$ after 48 h of transfection with either control (pcDNA3.1) or Htt (mHttex1) EGP-expressing construct. Values are represented as mean ± SD of four independent experiments. Ponceau red was used as total protein loading control. Unpaired t test, $^*p < 0.05$. (K) Immunoblottings of both GFP and actin in $STHdh^{7/7}$ cells after 48 h of transfection with either control (pcDNA3.1) or Htt (mHttex1) EGP-expressing construct.

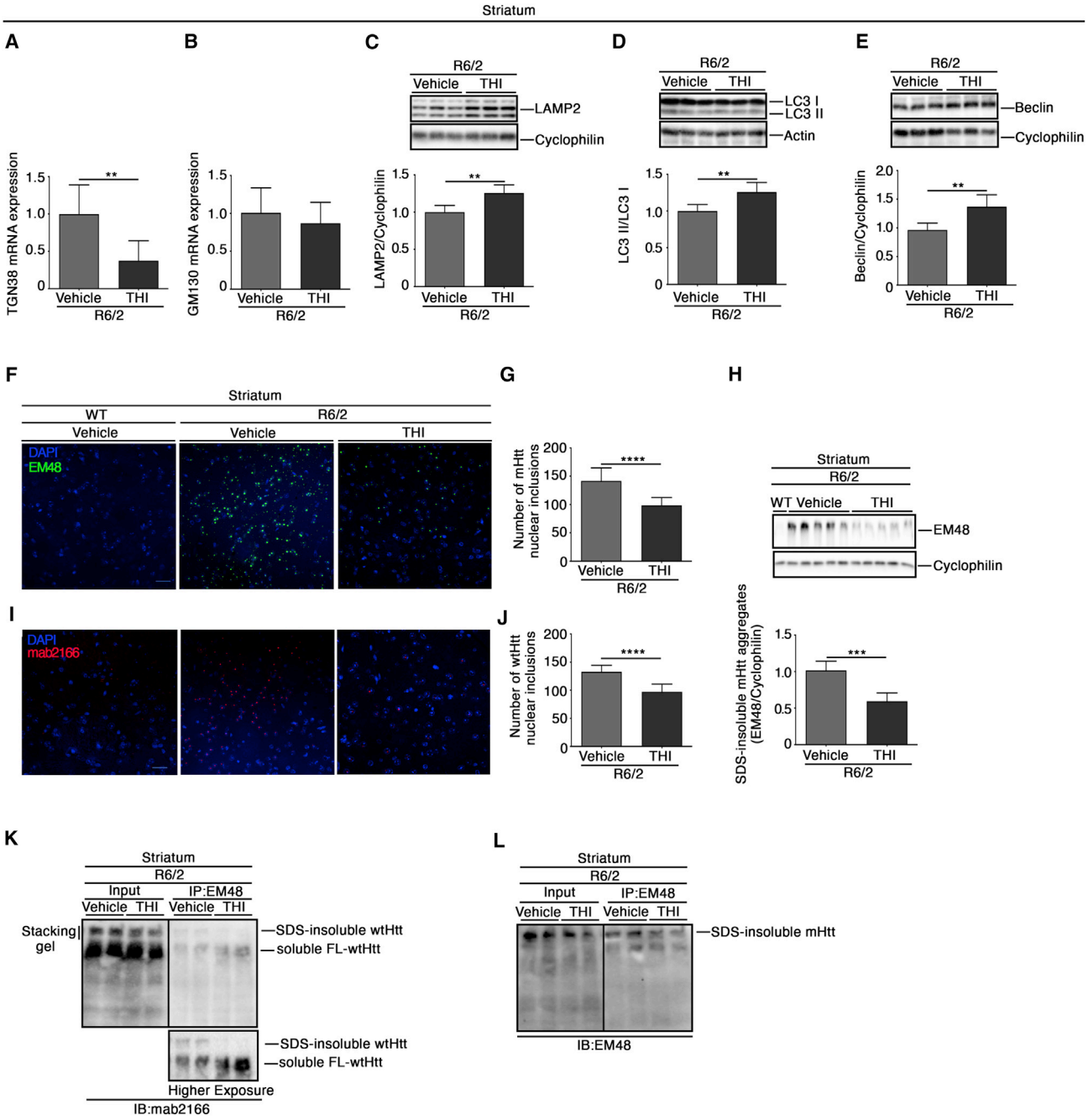

Figure 7. THI treatment modulates the expression of vesicle trafficking/autophagic markers and reduces Htt aggregation

(A) qPCR analysis of *trans*-GOLGI marker TGN38 in striatal tissues of vehicle- and THI-treated R6/2 mice at age 11 weeks. Values are represented as mean ± SD. N = 6 (females N = 3; males N = 3) for each group of mice. Unpaired t test, **p < 0.01. (B) qPCR analysis of *cis*-GOLGI marker GM130 in striatal tissues of vehicle- and THI-treated R6/2 mice at age 11 weeks. Values are represented as mean ± SD. N = 6 (females N = 3; males N = 3) for each group of mice. (C) Representative cropped immunoblotting and densitometric analysis of lysosomal marker LAMP2 in the striatum of vehicle- and THI-treated R6/2 mice at age 11 weeks. Values are represented as mean ± SD. N = 6 (females N = 3; males N = 3) for each group of mice. Unpaired t test, **p < 0.01. (D) Representative cropped immunoblotting and densitometric analysis of LC3II/LC3I in the striatum of vehicle- and THI-treated R6/2 mice at age 11 weeks. Values are represented as mean ± SD. N = 6 (females N = 3; males N = 3) for each group of mice. Unpaired t test, **p < 0.01. (E) Representative cropped immunoblotting and densitometric analysis of Beclin in the striatum of vehicle- and THI-treated R6/2 mice at age 11 weeks. Values are represented as mean ± SD. N = 6 (females N = 3; males N = 3) for each group of mice. Unpaired t test, **p < 0.01. (F) Representative fluorescence microscopy micrograph of EM48-positive mHtt nuclear inclusions (green signal) in the striatum of vehicle- and THI-treated R6/2 mice at age 11 weeks. Nuclei are stained with DAPI (blue

(legend continued on next page)

normalization of GluCer content. In this regard, in the context of HD, the stimulation of autophagic pathways may facilitate the reduction of Htt aggregates and eventually increase levels of "free" wt protein allowing the "re-establishment" of its physiological functions, eventually contributing to the maintenance of glycosphingolipid homeostasis through a possible positive feedback mechanism.

Evidence demonstrates that accumulation of GluCer is attributable to an abnormal endomembrane homeostasis and altered lipid recycling in different diseases.[81,82] We propose that such GluCer accumulation in HD may depend on the effect that mHtt has on the regulation of endomembrane and vesicle trafficking.[83,84]

In conclusion, our findings further support the concept that the alteration of (glyco)sphingolipid pathways may contribute to HD pathogenesis and may be eventually pharmacologically targeted. This is supported by the evidence that some drugs, including THI derivatives, whose molecular targets belong to these pathways, are already in clinical trial for different other diseases[85–88] and could be eventually repurposed for the treatment of HD and/or serve as a tool for the development of new ones.

MATERIALS AND METHODS

Animal models

All experimental procedures were approved by the IRCCS Neuromed Animal Care Review Board and by "Istituto Superiore di Sanità" (ISS permit numbers: 760/2020-PR and 433/2021-PR) and were conducted according to the 2010/63/EU directive for animal experiments.

Breeding pairs of the R6/2 line of transgenic mice (strain name: B6CBA-tgN (HDexon1) 62Gpb/1J) with ∼160 ± 10 (CAG) repeat expansions[89] were purchased from the Jackson Laboratories (Bar Harbor, ME). $Htt^{tmtm1Mfc}$/190tChdi (zQ175 knockin) mice (CAG198) were received from the CHDI Foundation by the Jackson Laboratories.

Heterozygous zQ175 knockin mice with ∼190 CAG repeats in a chimeric human/mouse exon 1 of the murine Htt gene[90] and age-matched WT littermates were used.

YAC128 expressing the entire human HD gene (including promoter region) with 128 CAG repeats. YAC128 mice and age-matched WT littermates were used, as described previously.[5]

Animal treatment

Analyses were carried out in both R6/2 mice and WT littermates starting from age 5 weeks. To ensure the homogeneity of experimental cohorts, mice from the same F generation were assigned to experimental groups, such that sex, age, and weight were matched.

In vivo drug administration

THI (Cayman, cat. no. 13,222) was dissolved in DMSO, further diluted in saline (vehicle) (100 μL total volume), and daily administered by i.p. injection at a dose of 0.1 mg/kg.[36] Control mice (WT and R6/2) were daily injected with the same volume of vehicle containing DMSO. The sites of injection were alternated between the right and left lower sides of mouse abdomen.

Clasping analysis

Clasping score was determined over 30 s. Mice were suspended by their tails at a height of 50 cm and a limb-clasping response was defined as the withdrawal of any limb to the torso for more than 2 s. The following scores were used: 0, absence of clasping; 0.5, withdrawal of any single limb; 1, withdrawal of any two limbs; 1.5, withdrawal of any three limbs; 2, withdrawal of all four limbs.

Motor behavior tests

Motor performance was assessed by horizontal ladder task and rotarod tests as described previously.[14] All tests were carried out blindly to the treatment.

Brain lysate preparation

Mice were sacrificed within 1 h after the last treatment by cervical dislocation and brains were removed from the skull, weighed, and bisected. Brains were immediately snap frozen in liquid N2 and pulverized in a mortar with a pestle, as described previously.[14]

Immunoblottings

Proteins (20 μg) were resolved on 10% SDS-PAGE and immunoblotted with the following antibodies: anti-DARPP-32 (1:1,000) (Cell Signaling, cat. no. 2302), anti-phospho-AKT (1:1,000) (Immunological Sciences, cat. no. AB-10521), anti-AKT (1:1,000) (Immunological Sciences, cat. no. MAB-94320), anti-BDNF (1:1,000) (Santa Cruz, cat. no. sc-546), anti-MBP (1:1,000) (Cell Signaling, cat. no. 13344), anti-MAG (1:1,000) (Santa Cruz, cat. no. sc-166849), anti-PSD-95 (1:1,000) (Millipore, cat. no. MAB1596), anti-$S1PR_1$ (1:1,000) (Immunological Sciences cat. no. AB-83739), $S1PR_5$ (1:1,000) (Immunological Sciences

signal). Scale bar, 20 μm. (G) Semiquantitative analysis of the number of mHtt nuclear inclusions. Data are represented as mean ± SD, N = 4 (females N = 2; males N = 2) for each group of mice. Unpaired t test, ****p < 0.0001. (H) Representative cropped immunoblotting of EM48-positive mHtt aggregates in striatal lysate of vehicle- and THI-treated R6/2 mice at age 11 weeks N = 6 (females N = 3; males N = 3) for each group of mice. Values are represented as mean ± SD. Unpaired t test, ***p < 0.001. (I) Representative fluorescence microscopy micrograph of mab2166-positive wtHtt nuclear inclusions (red signal) in the striatum of vehicle- and THI-treated R6/2 mice at age 11 weeks. Nuclei are stained with DAPI (blue signal). Scale bar, 20 μm. (J) Semiquantitative analysis of the number of wtHtt nuclear inclusions. Data are represented as mean ± SD, N = 4 (females N = 2; males N = 2) for each group of mice. Unpaired t test, ****p < 0.0001. (K) Immunoblotting analysis of both SDS-insoluble and soluble wtHtt, co-immunoprecipitated with EM48 antibody, and revealed with the anti-Htt mab2166. In each immunoblotting, all samples were run on the same gel. Non-adjacent samples were separated by a black line. (L) Immunoblotting analysis of both SDS-insoluble mHtt aggregates, co-immunoprecipitated and revealed with EM48 antibody. In each immunoblotting, all samples were run on the same gel. Non-adjacent samples are separated by a black line.

cat. no. AB-83741), anti-Htt (clone D7F7) (1:1,000) (Immunological Sciences, cat. no. MAB-94596), anti-GFP (1:2000) (Synaptic System, cat. no. 132 002), anti-LAMP2 (1:1,000) (Immunological Sciences, cat. no. AB-84316), anti-LC3B (1:1,000) (Sigma, cat. no. L7543), and anti-Beclin1 (1:1,000) (Santa Cruz, cat. no. sc-11427).

For protein normalization, anti-actin (1:5,000) (Sigma-Aldrich, cat. no. A5441), anti-cyclophilin (1:2,000) (Abcam, cat. no. ab16045), and/or anti-alpha-tubulin (1:2,000) (Abcam, cat. no. ab4074) were used. Immunoblots were then exposed to specific HRP-conjugated secondary antibodies (Millipore, cat. nos. 401315 and 401215). Protein bands were visualized by ECL and quantified by Image Lab Software (Bio-Rad Laboratories).

For the analysis of mHtt aggregates, protein lysates (30 μg) were resolved on 8% SDS-PAGE, the entire gel, including the stacking portion, was *trans*-blotted overnight at 250 mV in 0.05% SDS and 16% methanol-containing transfer buffer. Membrane was immunoblotted with anti-Htt (clone EM48) antibody (1:1,000) (Millipore, cat. no. MAB5374). A monoclonal anti-mouse HRP-conjugated antibody (Millipore, cat. no. 401215) was used as secondary antibody. Protein bands were visualized by ECL and quantified as described above.

Co-immunoprecipitations

Immunoprecipitation (1 mg total lysate) was performed using the anti-mHtt antibodies (clone EM48) complexed to protein G-Sepharose (Invitrogen, cat. no. 101243). The immunoprecipitated proteins were resolved on 7% SDS-PAGE, transferred overnight on a PVDF membrane, and detected by immunoblotting with mab2166 (1:1,000) (Millipore, cat. no. MAB2166) and EM48 (1:1,000). HRP-conjugated secondary antibodies (Millipore, cat. no. 401215) were used at 1:5,000 dilution. Protein bands were detected by ECL and visualized by Quantity One software (Bio-Rad Laboratories).

Histochemical analyses

Brains were processed, embedded in paraffin wax, and 10 μm coronal sections were cut using a microtome. Four mice/group were used, and immunostaining for mHtt and wtHtt aggregates was carried out using a mouse anti-mHtt antibody (clone EM48) (1:150) and a mouse anti-wtHtt antibody (mab2166) (1:150), as described recently.[14]

For analysis of the CC, four mice/group were analyzed. The thickness of the CC was measured in correspondence of the middle line of the brain as described previously.[43]

Transmission electron microscopy

Mouse brains were immersed in the fixing solution (paraformaldehyde 2.0% and glutaraldehyde 1% in 0.1 M phosphate buffer [pH 7.4]) overnight at 4°C. After washing in PBS (0.1 M), small blocks from the CC were dissected out and post-fixed in 1% osmium tetroxide for 1 h at 4°C. After washing in PBS, samples were dehydrated in a gradient of ethanol solutions and finally embedded in epon-araldite resin. Ultrathin sections (90 nm) were cut using an ultra-microtome (Leica Microsystems) to be collected on cupper grids and stained with uranyl acetate and lead citrate. Ultrathin sections were observed on electron microscopy (Jeol JEM SX100, Jeol, Tokyo, Japan) at an acceleration voltage of 80 kV. For ultrastructural morphometry, grids containing non-serial ultra-thin sections (90 nm thick) were examined at a magnification of 6,000×. Several grids were analyzed to count a total of 50 axons from the CC from each experimental group. For the ultrastructural analysis of axons, grids containing non-serial ultra-thin sections (90 nm thick) were examined at a magnification of 6,000×. Axon minimum and maximum diameter, axon mean diameter, and myelin thickness were assessed.

Whole-cell recordings from L5 pyramidal neurons

Mice were anesthetized and quickly decapitated, and the brain rapidly removed to ice-cold glycerol-based artificial cerebrospinal fluid (ACSF) containing the following (in mM): glycerol 250, KCl 2.5, $CaCl_2$ 2.4, $MgCl_2$ 1.2, NaH_2PO_4 1.2, $NaHCO_3$ 26, glucose 11, and Na pyruvate 0.1 [pH 7.35], aerated with 95% O_2/5% CO_2, 290–300 mOsm/L). Transversal slices, 350 μm in thickness, were cut with a vibratome (Leica VT 1000S) and placed in a slice incubation chamber at room temperature with oxygenated ACSF and transferred to a recording chamber within 1–6 h after slice preparation. Spontaneous EPSCs were recorded from L5 pyramidal neurons in the temporal cortex from 8-week-old mice. Recordings were performed at 22°C–25°C using a Multiclamp 700A amplifier (Axon Instruments, Foster City, CA) and −70 mV holding potential, in the presence of bicuculline 20 μM to block $GABA_A$ receptors.

The patch pipette (3–4 MΩ) was filled with the following solution (in mM): KCl 140, HEPES 10, 1,2-bis(2-aminophenoxy)ethane-N,N,N,N-tetra-acetic acid 5, $MgCl_2$ 2, MgATP 2 [pH 7.35], with KOH). ACSF had the following composition: 125 mM NaCl, 2.5 mM KCl, 2 mM $CaCl_2$, 1.25 mM NaH_2PO_4, 1 mM $MgCl_2$, 26 mM $NaHCO_3$, 10 mM glucose (pH 7.35).

Fly stocks

The fly strains used in this study were obtained from the Bloomington Stock Center: w*; P{UAS-HTT.128Q.FL}f27b, and w*; P{w[+mW.hs] = GawB}elav[C155]. Flies were reared on standard cornmeal-agar with a 12-h on-off light cycle at 22°C.

THI treatment and fly crosses

During the assays, flies were reared in tubes containing 2 mL of AF (2% agar, 10% powdered yeast, 10% sucrose, 0.1% nipagin) or on the same AF supplemented with THI. All tests were carried out blindly to the treatment.

THI was added onto the surface of AF at a final concentration of 50 μM, and left under gentle agitation for 3 h until dried. Controls were reared in AF supplemented with an equal quantity of PBS, devoid of THI. Expression of polyglutamine-containing human HTT was obtained through the bipartite expression system (UAS)-GAL4 in *trans*-heterozygous F1 progeny generated by crossing females carrying the pan-neural driver elav-Gal4 to males carrying

the UAS HTT128QFL construct at 27.5°C.[47] Only F1 adult females elav-GAL4/UAS HTT128QFL were used in this study.

Negative geotaxis assay

Negative geotaxis assay was carried out on F1 (Q128HD-FL) female flies on different days post eclosion, as described previously.[47] In brief, groups of 20 female flies were placed in a graduated empty plastic vial (18 × 2.5 cm) and allowed to recover for 30 min. Negative geotaxis was measured by recording the number of flies that climbed above the 10 cm mark within 20 s after a tap down of the flies to the bottom of the vial. This assay was repeated for the same group two times, allowing for a 4 min rest period between each trial. The number of flies per group that passed the 10 cm mark was recorded as a percentage of total flies. For each condition, 3 groups of 20 flies each were tested in the marked tube in 3 independent experiments, and the data were expressed as an average of the replicates ± SD (n = 180).

Lifespan analysis

Newly hatched F1 elav-GAL4/UAS HTT128QFL (Q128HD-FL) adult flies were collected, briefly anesthetized with CO_2, and sorted by sex. Five cohorts of 20 females were placed in vials containing AF, supplemented with or without THI, and reared at 27.5°C. They were transferred to new vials with fresh food every 2/3 days, and deaths were recorded at each transfer. The experiment ended when there were no more live flies in the vials. Lifespan was measured in two independent experiments (total n = 200) per treatment. Obtained values were used to calculate mean lifespan (mean survival days of all flies for each group), and maximum lifespan (maximum amount of days needed to reach 90% mortality).[91,92]

Mass spectrometry

Snap frozen brain tissues were transferred into glass tubes and stored at −80°C until lipid extraction. Lipids were extracted using a modified Bligh and Dyer method as described previously.[19] LC-MS/MS analyses of the samples were carried out on the Acquity UPLC system coupled with a Xevo TQ-MS triple-quadrupole mass spectrometer as described previously.[93]

Cell models

Conditionally immortalized mouse striatal knockin cells expressing endogenous levels of WT ($STHdh^{7/7}$) or mutant ($STHdh^{111/111}$) Htt were purchased from the Coriell Cell Repositories (Coriell Institute for Medical Research, Camden, NJ) and were maintained as described previously.[43]

Cell transfection

In both Htt siRNA and ectopic expression of EGFP-mHtt-exon1 experiments, STHdh cell lines were transiently transfected using Lipofectamine LTX and Plus reagent (Invitrogen, cat. no. 15338-100) and analyzed 48 h after transfection.

Cell lysate preparation

Cells lysates were prepared in lysis buffer containing 20 mM Tris (pH 7.4), 1% Nonidet P-40, 1 mM EDTA, 20 mM NaF, 2 mM Na_3VO_4, and 1:1,000 protease inhibitor mixture (Immunological Sciences, cat. no. IS11041), sonicated with 2 ×10 s pulses and then centrifuged for 10 min at 10,000 × *g*.

Semiquantitative analysis of glucosylceramide

Five micrograms of total protein lysate was spotted on nitrocellulose membrane using a slot-blotting apparatus (Hoefer PR 648 Slot Blot Blotting Manifold). Membranes were then blocked in 5% milk in TBS-T and incubated with anti-GluCer antibody[51] (1:1,000) (Glycobiotech, cat. no. RAS_0010). A polyclonal anti-rabbit HRP-conjugated antibody (Millipore, cat. no. 401315) was used as secondary antibody. Protein bands were visualized by ECL and quantified as reported above. Ponceau red staining served as a total protein loading control.[94]

Quantitative real-time PCR

Total RNA was extracted as described previously[15] and qPCR analysis was performed on a CFX Connect Real-Time System instrument (Bio-Rad Laboratories). The following primers were used (5′–>3′): CerS1-Fw: CACACATCTTTCGGCCCCT; CerS1-Rv: GCGGGTC ATGGAAGAAAGGA, CerS2-Fw: GGTGGAGGTAGACCTTTTGT CA; CerS2-Rv: CGGAACTTTTTGAGAAGACTGGG; Sptlc1-FW: TACTCAGAGACCTCCAGCTG; Sptlc1-RV: CACCAGGGATAT GCTGTCAT; Ugcg-FW: TTGTTCGGCTTGTGCTCTT; Ugcg-Rv: GAGACACCAGGGAGCTTGCT; Spns2-FW: TGAAGGCCCTGA TCCGAAAC; Spns2-RV: ATGAGGCTGTCTTTGGCTCC; Gba1-FW: CTTCCTATTTCAGGCGGTATCTT; Gba1-RV: AGAGTCAC AGTACGATGCATTA; Gba2-FW: CACCTATCTTGCCTCATGA CTAC; Gba2-RV: GAAACGTCCAGAGTCTCATCTC; TGN38-FW: GCAGCCACTTCTTTGCATATCTAG; TGN38-RV: AGTGAC TTTGGATCTTTTCCCTTC; GM-130 FW: CAGGCAGACAGGTA TAACAAG; GM130-RV: CGGAGTTTCTCTTCCAGTTC;

Cyc-Fw: TCCAAAGACAGCAGAAAACTTTCG; Cyc-Rv: TCTTCTTGCTGGT CTTGCCATTCC.

Statistics

Two-way ANOVA followed by Bonferroni post-test was used to compare treatment groups with the horizontal ladder task and rotarod tests as well as for the analysis of body weight gain. Mantel-Cox test was used for the fly lifespan. One-way ANOVA and two-tailed unpaired t test were used in all other experiments, as indicated.

All data were expressed as mean ± SD except in the electrophysiological studies and transmission electron microscopy analyses in which data were expressed as mean ± SEM.

SUPPLEMENTAL INFORMATION

Supplemental information can be found online at https://doi.org/10.1016/j.ymthe.2022.09.004.

ACKNOWLEDGMENTS

We thank Enrico Amico, Susy Giova, and Salvatore Castaldo for technical assistance. This study was funded by Telethon grant GGP20101

(to V.M.); by EHDN project no. 903 (to A.D.P.); by the "Deutsche Forschungsgemeinschaft" DFG project PA 1529/2-1 (to R.P.); and by NIH/NIEHS R01 ES016931 (to A.B.B.). This study was supported by Fondazione Neuromed.

AUTHOR CONTRIBUTIONS

V.M. and A.D.P. conceived the study and designed the experiments. G.P., L.C., F.M., N.R., P.L., K.M., T.F.B., T.J.B., P.S., and C.D.C. performed the experiments. A.A., A.B.B., F.A.D., S.F., F.F., and R.P. supervised the experiments and contributed to manuscript preparation. V.M., A.D.P., and G.P. wrote the manuscript.

DECLARATION OF INTERESTS

The authors declare no competing interests.

REFERENCES

1. Tabrizi, S.J., Flower, M.D., Ross, C.A., and Wild, E.J. (2020). Huntington disease: new insights into molecular pathogenesis and therapeutic opportunities. Nat. Rev. Neurol. *16*, 529–546.
2. Saudou, F., and Humbert, S. (2016). The biology of huntingtin. Neuron *89*, 910–926.
3. Chuang, C.L., and Demontis, F. (2021). Systemic manifestation and contribution of peripheral tissues to Huntington's disease pathogenesis. Ageing Res. Rev. *69*, 101358.
4. Wilton, D.K., and Stevens, B. (2020). The contribution of glial cells to Huntington's disease pathogenesis. Neurobiol. Dis. *143*, 104963.
5. Bichell, T.J.V., Wegrzynowicz, M., Tipps, K.G., Bradley, E.M., Uhouse, M.A., Bryan, M., Horning, K., Fisher, N., Dudek, K., Halbesma, T., et al. (2017). Reduced bioavailable manganese causes striatal urea cycle pathology in Huntington's disease mouse model. Biochim. Biophys. Acta Mol. Basis Dis. *1863*, 1596–1604.
6. Sbodio, J.I., Snyder, S.H., and Paul, B.D. (2018). Golgi stress response reprograms cysteine metabolism to confer cytoprotection in Huntington's disease. Proc. Natl. Acad. Sci. USA *115*, 780–785.
7. Singh, A., and Agrawal, N. (2022). Metabolism in Huntington's disease: a major contributor to pathology. Metab. Brain Dis. *37*, 1757–1771.
8. Maglione, V., Marchi, P., Di Pardo, A., Lingrell, S., Horkey, M., Tidmarsh, E., and Sipione, S. (2010). Impaired ganglioside metabolism in Huntington's disease and neuroprotective role of GM1. J. Neurosci. *30*, 4072–4080.
9. Di Pardo, A., Amico, E., and Maglione, V. (2016). Impaired levels of gangliosides in the corpus callosum of Huntington disease animal models. Front. Neurosci. *10*, 457.
10. Denny, C.A., Desplats, P.A., Thomas, E.A., and Seyfried, T.N. (2010). Cerebellar lipid differences between R6/1 transgenic mice and humans with Huntington's disease. J. Neurochem. *115*, 748–758.
11. Desplats, P.A., Denny, C.A., Kass, K.E., Gilmartin, T., Head, S.R., Sutcliffe, J.G., Seyfried, T.N., and Thomas, E.A. (2007). Glycolipid and ganglioside metabolism imbalances in Huntington's disease. Neurobiol. Dis. *27*, 265–277.
12. Hunter, M., Demarais, N.J., Faull, R.L.M., Grey, A.C., and Curtis, M.A. (2021). An imaging mass spectrometry atlas of lipids in the human neurologically normal and Huntington's disease caudate nucleus. J. Neurochem. *157*, 2158–2172.
13. Di Pardo, A., and Maglione, V. (2018). The S1P Axis: new exciting route for treating Huntington's disease. Trends Pharmacol. Sci. *39*, 468–480.
14. Di Pardo, A., Castaldo, S., Amico, E., Pepe, G., Marracino, F., Capocci, L., Giovannelli, A., Madonna, M., van Bergeijk, J., Buttari, F., et al. (2018). Stimulation of S1PR $_5$ with A-971432, a selective agonist, preserves blood-brain barrier integrity and exerts therapeutic effect in an animal model of Huntington's disease. Hum. Mol. Genet. *27*, 2490–2501.
15. Di Pardo, A., Pepe, G., Castaldo, S., Marracino, F., Capocci, L., Amico, E., Madonna, M., Giova, S., Jeong, S.K., Park, B.M., et al. (2019). Stimulation of sphingosine kinase 1 (SPHK1) is beneficial in a Huntington's disease pre-clinical model. Front. Mol. Neurosci. *12*, 100.
16. Moruno-Manchon, J.F., Uzor, N.E., Blasco-Conesa, M.P., Mannuru, S., Putluri, N., Furr-Stimming, E.E., and Tsvetkov, A.S. (2017). Inhibiting sphingosine kinase 2 mitigates mutant Huntingtin-induced neurodegeneration in neuron models of Huntington disease. Hum. Mol. Genet. *26*, 1305–1317.
17. Pirhaji, L., Milani, P., Dalin, S., Wassie, B.T., Dunn, D.E., Fenster, R.J., Avila-Pacheco, J., Greengard, P., Clish, C.B., Heiman, M., et al. (2017). Identifying therapeutic targets by combining transcriptional data with ordinal clinical measurements. Nat. Commun. *8*, 623.
18. Di Pardo, A., Basit, A., Armirotti, A., Amico, E., Castaldo, S., Pepe, G., Marracino, F., Buttari, F., Digilio, A.F., and Maglione, V. (2017). De novo synthesis of sphingolipids is defective in experimental models of Huntington's disease. Front. Neurosci. *11*, 698.
19. Di Pardo, A., Amico, E., Basit, A., Armirotti, A., Joshi, P., Neely, M.D., Vuono, R., Castaldo, S., Digilio, A.F., Scalabrì, F., et al. (2017). Defective Sphingosine-1-phosphate metabolism is a druggable target in Huntington's disease. Sci. Rep. *7*, 5280.
20. Pirhaji, L., Milani, P., Leidl, M., Curran, T., Avila-Pacheco, J., Clish, C.B., White, F.M., Saghatelian, A., and Fraenkel, E. (2016). Revealing disease-associated pathways by network integration of untargeted metabolomics. Nat. Methods *13*, 770–776.
21. Grassi, S., Mauri, L., Prioni, S., Cabitta, L., Sonnino, S., Prinetti, A., and Giussani, P. (2019). Sphingosine 1-phosphate receptors and metabolic enzymes as druggable targets for brain diseases. Front. Pharmacol. *10*, 807.
22. Ayub, M., Jin, H.K., and Bae, J.S. (2021). Novelty of sphingolipids in the central nervous system physiology and disease: focusing on the sphingolipid hypothesis of neuroinflammation and neurodegeneration. Int. J. Mol. Sci. *22*, 7353.
23. Van Echten-Deckert, G., Hagen-Euteneuer, N., Karaca, I., and Walter, J. (2014). Sphingosine-1-phosphate: boon and bane for the brain. Cell. Physiol. Biochem. *34*, 148–157.
24. Maceyka, M., Harikumar, K.B., Milstien, S., and Spiegel, S. (2012). Sphingosine-1-phosphate signaling and its role in disease. Trends Cell Biol. *22*, 50–60.
25. Serra, M., and Saba, J.D. (2010). Sphingosine 1-phosphate lyase, a key regulator of sphingosine 1-phosphate signaling and function. Adv. Enzyme Regul. *50*, 349–362.
26. Blaho, V.A. (2020). Druggable sphingolipid pathways: experimental models and clinical opportunities. Adv. Exp. Med. Biol. *1274*, 101–135.
27. Hagen, N., Hans, M., Hartmann, D., Swandulla, D., and Van Echten-Deckert, G. (2011). Sphingosine-1-phosphate links glycosphingolipid metabolism to neurodegeneration via a calpain-mediated mechanism. Cell Death Differ. *18*, 1356–1365.
28. Hagen, N., Van Veldhoven, P.P., Proia, R.L., Park, H., Merrill, A.H., and Van Echten-Deckert, G. (2009). Subcellular origin of sphingosine 1-phosphate is essential for its toxic effect in lyase-deficient neurons. J. Biol. Chem. *284*, 11346–11353.
29. Alam, S., Piazzesi, A., Abd El Fatah, M., Raucamp, M., and van Echten-Deckert, G. (2020). Neurodegeneration caused by S1P-lyase deficiency involves calcium-dependent tau pathology and abnormal histone acetylation. Cells *9*, 2189.
30. Mitroi, D.N., Deutschmann, A.U., Raucamp, M., Karunakaran, I., Glebov, K., Hans, M., Walter, J., Saba, J., Gräler, M., Ehninger, D., et al. (2016). Sphingosine 1-phosphate lyase ablation disrupts presynaptic architecture and function via an ubiquitin- proteasome mediated mechanism. Sci. Rep. *6*, 37064.
31. Mitroi, D.N., Karunakaran, I., Gräler, M., Saba, J.D., Ehninger, D., Ledesma, M.D., and van Echten-Deckert, G. (2017). SGPL1 (sphingosine phosphate lyase 1) modulates neuronal autophagy via phosphatidylethanolamine production. Autophagy *13*, 885–899.
32. Billich, A., Baumruker, T., Beerli, C., Bigaud, M., Bruns, C., Calzascia, T., Isken, A., Kinzel, B., Loetscher, E., Metzler, B., et al. (2013). Partial deficiency of sphingosine-1-phosphate lyase confers protection in experimental autoimmune encephalomyelitis. PLoS One *8*, e59630.
33. Vollmuth, T.A. (2018). Caramel color safety - an update. Food Chem. Toxicol. *111*, 578–596.
34. Moruno Manchon, J.F., Uzor, N.E., Dabaghian, Y., Furr-Stimming, E.E., Finkbeiner, S., and Tsvetkov, A.S. (2015). Cytoplasmic sphingosine-1-phosphate pathway modulates neuronal autophagy. Sci. Rep. *5*, 15213.
35. Nguyen-Tran, D.H., Hait, N.C., Sperber, H., Qi, J., Fischer, K., Ieronimakis, N., Pantoja, M., Hays, A., Allegood, J., Reyes, M., et al. (2014). Molecular mechanism of sphingosine-1-phosphate action in Duchenne muscular dystrophy. Dis. Model. Mech. *7*, 41–54.

36. Gobin, S.J., and Phillips, J.A. (1991). Immunosuppressive effects of 2-acetyl-4-tetrahydroxybutyl imidazole (THI) in the rat. Clin. Exp. Immunol. *85*, 335–340.

37. Matamales, M., Bertran-Gonzalez, J., Salomon, L., Degos, B., Deniau, J.M., Valjent, E., Hervé, D., and Girault, J.A. (2009). Striatal medium-sized spiny neurons: identification by nuclear staining and study of neuronal subpopulations in BAC transgenic mice. PLoS One *4*, e4770.

38. Ehrlich, M.E. (2012). Huntington's disease and the striatal medium spiny neuron: cell-autonomous and non-cell-autonomous mechanisms of disease. Neurotherapeutics *9*, 270–284.

39. Di Paola, M., Phillips, O.R., Sanchez-Castaneda, C., Di Pardo, A., Maglione, V., Caltagirone, C., Sabatini, U., and Squitieri, F. (2014). MRI measures of corpus callosum iron and myelin in early Huntington's disease. Hum. Brain Mapp. *35*, 3143–3151.

40. Gatto, R.G., Weissmann, C., Amin, M., Angeles-López, Q.D., García-Lara, L., Castellanos, L.C.S., Deyoung, D., Segovia, J., Mareci, T.H., Uchitel, O.D., and Magin, R.L. (2021). Evaluation of early microstructural changes in the R6/1 mouse model of Huntington's disease by ultra-high field diffusion MR imaging. Neurobiol. Aging *102*, 32–49.

41. Estevez-Fraga, C., Scahill, R., Rees, G., Tabrizi, S.J., and Gregory, S. (2020). Diffusion imaging in Huntington's disease: comprehensive review. J. Neurol. Neurosurg. Psychiatry *92*, 62–69.

42. Dumas, E.M., Van Den Bogaard, S.J.A., Ruber, M.E., Reilman, R.R., Stout, J.C., Craufurd, D., Hicks, S.L., Kennard, C., Tabrizi, S.J., Van Buchem, M.A., et al. (2012). Early changes in white matter pathways of the sensorimotor cortex in premanifest Huntington's disease. Hum. Brain Mapp. *33*, 203–212.

43. Di Pardo, A., Amico, E., Favellato, M., Castrataro, R., Fucile, S., Squitieri, F., and Maglione, V. (2014). FTY720 (fingolimod) is a neuroprotective and disease-modifying agent in cellular and mouse models of huntington disease. Hum. Mol. Genet. *23*, 2251–2265.

44. Kim, E., and Sheng, M. (2004). PDZ domain proteins of synapses. Nat. Rev. Neurosci. *5*, 771–781.

45. Won, S., Incontro, S., Nicoll, R.A., and Roche, K.W. (2016). PSD-95 stabilizes NMDA receptors by inducing the degradation of STEP61. Proc. Natl. Acad. Sci. USA *113*, E4736–E4744.

46. Marsh, J.L., Pallos, J., and Thompson, L.M. (2003). Fly models of Huntington's disease. Hum. Mol. Genet. *12*, R187–R193.

47. Di Cristo, F., Calarco, A., Digilio, F.A., Sinicropi, M.S., Rosano, C., Galderisi, U., Melone, M.A.B., Saturnino, C., and Peluso, G. (2020). The discovery of highly potent THP derivatives as OCTN2 inhibitors: from structure-based virtual screening to in vivo biological activity. Int. J. Mol. Sci. *21*, 74311.

48. Baranowska, U., Holownia, A., Chabowski, A., and Baranowski, M. (2020). Pharmacological inhibition of sphingosine-1-phosphate lyase partially reverses spatial memory impairment in streptozotocin-diabetic rats. Mol. Cell. Neurosci. *107*, 103526.

49. Gorshkova, I.A., Wang, H., Orbelyan, G.A., Goya, J., Natarajan, V., Beiser, D.G., Vanden Hoek, T.L., and Berdyshev, E.V. (2013). Inhibition of sphingosine-1-phosphate lyase rescues sphingosine kinase-1-knockout phenotype following murine cardiac arrest. Life Sci. *93*, 359–366.

50. Yu, X.Q., Kramer, J., Moran, L., O'Neill, E., Nouraldeen, A., Oravecz, T., and Wilson, A.G.E. (2010). Pharmacokinetic/pharmacodynamic modelling of 2-acetyl-4(5)-tetrahydroxybutyl imidazole-induced peripheral lymphocyte sequestration through increasing lymphoid sphingosine 1-phosphate. Xenobiotica *40*, 350–356. https://doi.org/10.3109/00498251003611376.

51. D'Angelo, G., Polishchuk, E., Di Tullio, G., van der Spoel, A.C., Santoro, M., Di Campli, A., Godi, A., West, G., Bielawski, J., et al. (2007). Glycosphingolipid synthesis requires FAPP2 transfer of glucosylceramide. Nature *449*, 62–67.

52. Futerman, A.H., and Platt, F.M. (2017). The metabolism of glucocerebrosides - from 1965 to the present. Mol. Genet. Metab. *120*, 22–26.

53. Futerman, A.H. (2006). Intracellular trafficking of sphingolipids: relationship to biosynthesis. Biochim. Biophys. Acta *1758*, 1885–1892.

54. Lippincott-Schwartz, J., and Phair, R.D. (2010). Lipids and cholesterol as regulators of traffic in the endomembrane system. Annu. Rev. Biophys. *39*, 559–578.

55. Holthuis, J.C., Pomorski, T., Raggers, R.J., Sprong, H., and Van Meer, G. (2001). The organizing potential of sphingolipids in intracellular membrane transport. Physiol. Rev. *81*, 1689–1723.

56. Morell, C., Bort, A., Vara-Ciruelos, D., Ramos-Torres, Á., Altamirano-Dimas, M., Díaz-Laviada, I., and Rodríguez-Henche, N. (2016). Up-regulated expression of LAMP2 and autophagy activity during neuroendocrine differentiation of prostate cancer LNCaP cells. PLoS One *11*, e0162977.

57. Saftig, P., and Klumperman, J. (2009). Lysosome biogenesis and lysosomal membrane proteins: trafficking meets function. Nat. Rev. Mol. Cell Biol. *10*, 623–635.

58. Loeffler, D.A. (2019). Influence of normal aging on brain autophagy: a complex scenario. Front. Aging Neurosci. *11*, 49.

59. Jarosińska, O.D., and Rüdiger, S.G.D. (2021). Molecular strategies to target protein aggregation in Huntington's disease. Front. Mol. Biosci. *8*, 769184.

60. Reiner, A., Dragatsis, I., and Dietrich, P. (2011). Genetics and neuropathology of Huntington's disease. Int. Rev. Neurobiol. *98*, 325–372.

61. Cattaneo, E., Rigamonti, D., Goffredo, D., Zuccato, C., Squitieri, F., and Sipione, S. (2001). Loss of normal huntingtin function: new developments in Huntington's disease research. Trends Neurosci. *24*, 182–188.

62. Kim, S., and Kim, K.-T. (2014). Therapeutic approaches for inhibition of protein aggregation in Huntington's disease. Exp. Neurobiol. *23*, 36–44.

63. Li, L., Liu, H., Dong, P., Li, D., Legant, W.R., Grimm, J.B., Lavis, L.D., Betzig, E., Tjian, R., and Liu, Z. (2016). Real-time imaging of Huntingtin aggregates diverting target search and gene transcription. Elife *5*, e17056.

64. Narain, Y., Wyttenbach, A., Rankin, J., Furlong, R.A., and Rubinsztein, D.C. (1999). A molecular investigation of true dominance in Huntington's disease. J. Med. Genet. *36*, 739–746.

65. Nucifora, F.C., Jr., Sasaki, M., Peters, M.F., Huang, H., Cooper, J.K., Yamada, M., Takahashi, H., Tsuji, S., Troncoso, J., Dawson, V.L., et al. (2001). Interference by huntingtin and atrophin-1 with cbp-mediated transcription leading to cellular toxicity. Science *291*, 2423–2428.

66. Riguet, N., Mahul-Mellier, A.L., Maharjan, N., Burtscher, J., Croisier, M., Knott, G., Hastings, J., Patin, A., Reiterer, V., Farhan, H., et al. (2021). Nuclear and cytoplasmic huntingtin inclusions exhibit distinct biochemical composition, interactome and ultrastructural properties. Nat. Commun. *12*, 6579.

67. Wheeler, V.C., White, J.K., Gutekunst, C.A., Vrbanac, V., Weaver, M., Li, X.J., Li, S.H., Yi, H., Vonsattel, J.P., Gusella, J.F., et al. (2000). Long glutamine tracts cause nuclear localization of a novel form of huntingtin in medium spiny striatal neurons in HdhQ92 and HdhQ111 knock-in mice. Hum. Mol. Genet. *9*, 503–513.

68. Fodale, V., Pintauro, R., Daldin, M., Altobelli, R., Spiezia, M.C., Bisbocci, M., Macdonald, D., and Bresciani, A. (2020). Analysis of mutant and total huntingtin expression in Huntington's disease murine models. Sci. Rep. *10*, 22137.

69. Hensman Moss, D.J., Robertson, N., Farmer, R., Scahill, R.I., Haider, S., Tessari, M.A., Flynn, G., Fischer, D.F., Wild, E.J., Macdonald, D., and Tabrizi, S.J. (2017). Quantification of huntingtin protein species in Huntington's disease patient leukocytes using optimised electrochemiluminescence immunoassays. PLoS One *12*, e0189891.

70. Cong, S.Y., Pepers, B.A., Roos, R.A.C., Van Ommen, G.J.B., and Dorsman, J.C. (2005). Epitope mapping of monoclonal antibody 4C8 recognizing the protein huntingtin. Hybridoma *24*, 231–235.

71. Guo, S., Yu, Y., Zhang, N., Cui, Y., Zhai, L., Li, H., Zhang, Y., Li, F., Kan, Y., and Qin, S. (2014). Higher level of plasma bioactive molecule sphingosine 1-phosphate in women is associated with estrogen. Biochim. Biophys. Acta *1841*, 836–846.

72. Gu, X., Jiang, Y., Xue, W., Song, C., Wang, Y., Liu, Y., and Cui, B. (2019). SPNS2 promotes the malignancy of colorectal cancer cells via regulating Akt and ERK pathway. Clin. Exp. Pharmacol. Physiol. *46*, 861–871.

73. Akhter, M.Z., Chandra Joshi, J., Balaji Ragunathrao, V.A., Maienschein-Cline, M., Proia, R.L., Malik, A.B., and Mehta, D. (2021). Programming to S1PR1^{+} endothelial cells promotes restoration of vascular integrity. Circ. Res. *129*, 221–236.

74. Zulueta, A., Dei Cas, M., Luciano, F., Mingione, A., Pivari, F., Righi, I., Morlacchi, L., Rosso, L., Signorelli, P., Ghidoni, R., et al. (2021). Spns2 transporter contributes to the accumulation of S1P in cystic fibrosis human bronchial epithelial cells. Biomedicines *9*, 1121.

75. Di Pardo, A., Pepe, G., Capocci, L., Marracino, F., Amico, E., Del Vecchio, L., Giova, S., Jeong, S.K., Park, B.M., Park, B.D., and Maglione, V. (2020). Treatment with K6PC-5, a selective stimulator of SPHK1, ameliorates intestinal homeostasis in an animal model of Huntington's disease. Neurobiol. Dis. *143*, 105009.

76. Indellicato, R., and Trinchera, M. (2019). The link between gaucher disease and Parkinson's disease sheds light on old and novel disorders of sphingolipid metabolism. Int. J. Mol. Sci. *20*, E3304.

77. Bouscary, A., Quessada, C., René, F., Spedding, M., Turner, B.J., Henriques, A., Ngo, S.T., and Loeffler, J.P. (2021). Sphingolipids metabolism alteration in the central nervous system: amyotrophic lateral sclerosis (ALS) and other neurodegenerative diseases. Semin. Cell Dev. Biol. *112*, 82–91.

78. Do, J., McKinney, C., Sharma, P., and Sidransky, E. (2019). Glucocerebrosidase and its relevance to Parkinson disease. Mol. Neurodegener. *14*, 36.

79. Henriques, A., Croixmarie, V., Priestman, D.A., Rosenbohm, A., Dirrig-Grosch, S., D'Ambra, E., Huebecker, M., Hussain, G., Boursier-Neyret, C., Echaniz-Laguna, A., et al. (2015). Amyotrophic lateral sclerosis and denervation alter sphingolipids and up-regulate glucosylceramide synthase. Hum. Mol. Genet. *24*, 7390–7405.

80. Dodge, J.C., Treleaven, C.M., Pacheco, J., Cooper, S., Bao, C., Abraham, M., Cromwell, M., Sardi, S.P., Chuang, W.L., Sidman, R.L., et al. (2015). Glycosphingolipids are modulators of disease pathogenesis in amyotrophic lateral sclerosis. Proc. Natl. Acad. Sci. USA *112*, 8100–8105.

81. Parenti, G., Medina, D.L., and Ballabio, A. (2021). The rapidly evolving view of lysosomal storage diseases. EMBO Mol. Med. *13*, e12836.

82. Abdul-Hammed, M., Breiden, B., Schwarzmann, G., and Sandhoff, K. (2017). Lipids regulate the hydrolysis of membrane bound glucosylceramide by lysosomal β-glucocerebrosidase. J. Lipid Res. *58*, 563–577.

83. Caviston, J.P., and Holzbaur, E.L.F. (2009). Huntingtin as an essential integrator of intracellular vesicular trafficking. Trends Cell Biol. *19*, 147–155.

84. Wanker, E.E., Ast, A., Schindler, F., Trepte, P., and Schnoegl, S. (2019). The pathobiology of perturbed mutant huntingtin protein-protein interactions in Huntington's disease. J. Neurochem. *151*, 507–519.

85. O'Sullivan, S., and Dev, K.K. (2017). Sphingosine-1-phosphate receptor therapies: advances in clinical trials for CNS-related diseases. Neuropharmacology *113*, 597–607.

86. Chew, W.S., Wang, W., and Herr, D.R. (2016). To fingolimod and beyond: the rich pipeline of drug candidates that target S1P signaling. Pharmacol. Res. *113*, 521–532.

87. Canals, D., and Clarke, C.J. (2022). Compartmentalization of Sphingolipid metabolism: implications for signaling and therapy. Pharmacol. Ther. *232*, 108005.

88. Nabizadeh, A., Amani, B., Kadivar, M., Toroski, M., Asl, A.A., Bayazidi, Y., Mojahedian, M., and Davari, M. (2018). The clinical efficacy of imiglucerase versus eliglustat in patients with gaucher's disease type 1: a systematic review. J. Res. Pharm. Pract. *7*, 171–177.

89. Mangiarini, L., Sathasivam, K., Seller, M., Cozens, B., Harper, A., Hetherington, C., Lawton, M., Trottier, Y., Lehrach, H., Davies, S.W., and Bates, G.P. (1996). Exon 1 of the HD gene with an expanded CAG repeat is sufficient to cause a progressive neurological phenotype in transgenic mice. Cell *87*, 493–506.

90. Menalled, L.B., Kudwa, A.E., Miller, S., Fitzpatrick, J., Watson-Johnson, J., Keating, N., Ruiz, M., Mushlin, R., Alosio, W., McConnell, K., et al. (2012). Comprehensive behavioral and molecular characterization of a new knock-in mouse model of Huntington's disease: zQ175. PLoS One *7*, e49838.

91. Bovier, T.F., Rossi, S., Mita, D.G., and Digilio, F.A. (2018). Effects of the synthetic estrogen 17-α-ethinylestradiol on Drosophila melanogaster: dose and gender dependence. Ecotoxicol. Environ. Saf. *162*, 625–632.

92. Bovier, T.F., Cavaliere, D., Colombo, M., Peluso, G., Giordano, E., and Digilio, F.A. (2019). Methods to test endocrine disruption in Drosophila melanogaster. J. Vis. Exp. e59535.

93. Basit, A., Piomelli, D., and Armirotti, A. (2015). Rapid evaluation of 25 key sphingolipids and phosphosphingolipids in human plasma by LC-MS/MS. Anal. Bioanal. Chem. *407*, 5189–5198.

94. Di Pardo, A., Alberti, S., Maglione, V., Amico, E., Cortes, E.P., Elifani, F., Battaglia, G., Busceti, C.L., Nicoletti, F., Vonsattel, J.P.G., and Squitieri, F. (2013). Changes of peripheral TGF-β1 depend on monocytes-derived macrophages in Huntington disease. Mol. Brain *6*, 55.